The Seesaw Mechanism Legacy, The root of Neutrino Masses and Leptogenesis

Albert Forsyth Daneri

In partial fulfillment of the requirements for the degree
MSc Quantum Fields and Fundamental Forces
at Imperial College London

London, England

September 2023

Supervisor Prof. Arttu Rajantie

Abstract

This investigation studied the Type I, Type II and Type III Seesaw Mechanisms in relation to the neutrino mass problem and the Universe's Baryon Asymmetry (Leptogenesis). The Type I Seesaw included heavy right-handed neutrinos to the SM. The Type II Seesaw incorporated a Higgs triplet, and finally, the Type III Seesaw introduced new left-handed fermions. In addition, The Type I and Type III Seesaw Models explain Leptogenesis through the decay of new right-handed neutrinos and new fermions, respectively. In contrast, the Type II Seesaw Model has been shown recently to explain the asymmetry through the Afflect-Dine Mechanism. Collider and low energy (charge lepton flavour violation) experiments are testing for the signature of Leptogenesis successful seesaw extensions to the SM. The sensitives of current muon decay searches for a three right-handed quasi-degenerate neutrino Type I Low Scale Seesaw and a Type II Seesaw were examined. In addition, searches for a Type II Seesaw in collider experiments were investigated. Future investigations on Low-Scale Seesaws are shown to be promising.

Acknowledgements

I want to thank my supervisor, Prof Arttu Rajantie, for his guidance in the project and my family for all their encouragement throughout my degree. Further, I want to thank my friends Sunny and Andres for our constant laughs throughout this year and their support.

Contents

Chapter 1

Introduction

The Standard Model (SM) is a widely accepted theory in particle physics that describes three of nature's four fundamental forces [1]. The model provides an understanding of the origin of particles and the nature of their interactions through symmetries. In 1964, Peter Higgs and five other physicists postulated the Higgs Mechanism to complete the SM and resolve the inconsistency between the predicted mass of Z and W bosons and their experimental value [2] [3] [4]. Later, in 2012, the Higgs Boson was detected in CERN's Large Hadron Collider (LHC), and the Higgs field was proved to exist [5]. Even though the central problem was resolved, there are still various fundamental problems that the SM can not settle.

The current SM predicts that neutrinos are massless, which is inconsistent with recent experimental data. Before discovering the Higgs field in 1968, Bruno Pontecorvo predicted that neutrinos were massive particles with oscillating flavours [6]. This phenomenon was later observed in several experiments, particularly Super-Kamiokande (SK) [7], Homestake [8], and the Sudbury Neutrino Observatory (SNO) [9], thus proving the SM is incomplete. The first proposed solution to this problem, the "Dirac" neutrino option, is to consider the neutrino like the other particles in the SM, generating mass through the Higgs Mechanism [10]. But, its right-handed state would not interact with other SM particles. The second solution, the "Majorana" neutrino option, uses the Majorana equation, which requires the neutrino and its antiparticle to be the same. The SM could then be extended through Seesaw mechanisms. There has yet to be confirmation for either of the solutions. Therefore, many modern experiments have been designed to test these particles and constrain their parameters.

The "Majorana" option opens many possibilities for extending the SM, i.e. the Type I, II, and III Seesaw Mechanisms. In the Type I Seesaw Model, heavy right-handed neutrinos (RHN) are added to the SM [10], including a Majorana mass term and new Yukawa interaction with the SM Higgs. Then, in the Type II Seesaw Model [11], the SM scalar sector is expanded by the addition of a $SU(2)_L$ triplet scalar (A Higgs triplet), which leads to, particularly, a new Yukawa term between the scalar and the lepton doublet. Finally, the Type III Seesaw Model introduces three left-handed (LH) triplets of leptons [12], which add a series of interactions and mass terms.

The addition of a Seesaw mechanism explicitly shows how the mass of the neutrinos can be generated. Additionally, it implicitly explains the baryon asymmetry of the universe through Leptogenesis. In brief, in Leptogenesis, heavy leptons (i.e. heavy neutrinos, heavy fermions) in the early universe decayed into an asymmetry or, through the Afflect-Dine mechanism, evolved into a lepton asymmetry, which then was transferred into baryons through a sphaleron process [10] [11] [12]. The requirement for Leptogenesis reflects constraints on the parameters of Seesaw models, which can be tested.

The most widely studied model is the Type I Seesaw, which is problematic to study at high energies as RH neutrino masses are beyond the reach of current and future colliders [13]. However, in low-scale Type I Seesaw Models, the neutrino mass can be sub-TeV scale through resonant Leptogenesis or Leptogenesis through neutrino oscillations [14]. It thus can be probed in low-energy experiments such as future μ decay (e.g. MEG, Mu2e, COMET).

The Type II Seesaw has been shown to cause Leptogenesis through the Afflect-Dine Mechanism effectively [11]. The inclusion of a triplet Higgs to the SM leads to 6 additional scalars, such as the singly charged Higgs and the doubly charged Higgs, which can be searched for in collider experiments [15]. Furthermore, if the scalar is added, the new interactions will affect charged and neutral currents, thus affecting μ decays [16]. One can draw limits for the Yukawa matrix from future muon decay experiments.

This investigation aims at studying the suggested solutions to the neutrino mass problem and the BAU. Further, to investigate the relevance of charged lepton flavour violating (cLFV) decays and scalar triplet decays to signatures of Leptogenesis. The status and sensitivities of current muon decay searches were examined.

Chapter 2

Neutrino Masses

In the past, SM neutrinos were modelled as massless since the neutrino mass limits were directly measured to be consistent with zero (due to their minuteness). However, in 1998, neutrino oscillations between flavour states were discovered, implying that they consist of a mix of mass states [7]. The three neutrino flavours, which interact weakly with charged leptons, are each a different superposition of three mass eigenstates. As these superpositions propagate through space, the phases of each state advance at different rates due to slight mass differences. Labelling the three mass states as ν_1, ν_2, ν_3, and assuming they have different masses, with U_{ei} as the relevant PMNS mixing matrix element [17]. Whenever one creates an electron in β decay, a coherent superposition of ν_i is created. This superposition is denoted as the electron neutrino,

$$\big|\nu_e\big\rangle = U_{e1}\big|\nu_1\big\rangle + U_{e2}\big|\nu_2\big\rangle + U_{e3}\big|\nu_3\big\rangle. \tag{2.1}$$

For this reason, if a neutrino is created at the source, the phase between the mass states will change as they travel through space to the detector. When detected, the relative phases between the mass eigenstates will change. Thus, detecting a different flavour than the one produced is possible. Restricting to two flavour oscillations (2 mass state system) [7], the probability of starting at a flavour ν_α and detecting ν_β is

$$P(v_\alpha \to v_\beta) = \sin^2(2\theta)\sin^2(1.27\frac{\Delta m^2 L(km)}{E(GeV)}). \tag{2.2}$$

Here, θ (the mixing angle) measures how different the flavour states are compared to the mass states. L/E is the ratio between the distance from the detector to the source and the particle's energy. The mass squared difference, $\Delta m^2 = m_1^2 - m_2^2$, is the difference of the squared masses of the individual mass states. Thus, neutrinos must carry mass, and the mass of each mass eigenstate must be different for a non-zero probability.

2.1 Evidence of Neutrino Oscillations and Mass Hierarchy

Cosmic ray collisions in the atmosphere produce hadronic showers, which subsequently provoke the creation of atmospheric neutrinos. In this system, the creation of electron and muon neutrinos (v_e and v_u, respectively) is dominated by the following reactions and their charge conjugates [7]:

$$\pi^+ \to \mu^+ + v_\mu, \quad \mu^+ \to e^+ + \overline{v_\mu} + v_e, \tag{2.3}$$

where π is a pion, and μ is a muon. These reactions give an predicted ratio, v_μ/v_e, of the flux of $v_\mu + \overline{v_\mu}$ to the flux of $v_e + \overline{v_e}$ of roughly 2 [7]. Experiments deep beneath the ground measure this ratio by detecting the final state of leptons generated through neutrino's charged-current interactions. Then, the lepton of the final state is used to identify the neutrino flavour.

Since 1985, SK has been an experiment aimed at searching for atmospheric neutrino oscillations through Cherenkov radiation. The detector consists of a 50 kton cylinder filled with pure water, and it is located 1km underground in the Kamioka mine (to shield against other particles) [18]. Figure 2.1 shows the confidence levels (CL) of the SK results from 1998, which overlaps with the CL of the Kamiokande (K) experiment. The SK region was shown to favour lower values of mass squared difference than allowed by K. The SK result was shown to agree with the two-flavour oscillation model for $v_\mu \Longleftrightarrow v_\tau$ (where v_τ is the tau neutrino, equation 2.2) with fitting parameters of $\sin^2 2\theta > 0.82$ and $5 \times 10^{-4} < \Delta m^2 < 6 \times 10^{-3} eV^2$ at 90% CL [7]. Since then, other experiments have independently arrived at an equivalent result, including Homestake [8] and SNO [9]. Therefore, the finding of neutrino oscillations confirmed that neutrinos have mass, and a Nobel Prize was granted to Takaaki Kajita and Arthur B. McDonald in 2015 for the discovery [19].

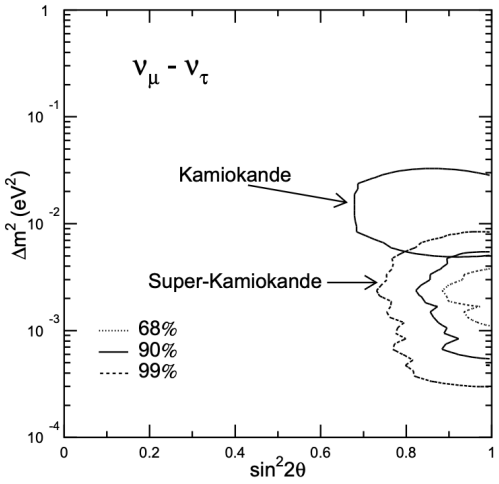

Figure 2.1: The graph shows the 68%, 90% and 99% CL for $sin^2(2\theta)$ and Δm^2 for υ_μ-υ_τ two-neutrino oscillations from the SK experiment. The 90% CL from the Kamiokande experiment is also shown [7].

As demonstrated in equation 2.2, through neutrino oscillations, one can only measure the mass squared difference between states. Thus, currently, there is no consensus whether ν_3 neutrino mass eigenstates are heavier or lighter than ν_1 and ν_2 neutrino mass eigenstates (equation 2.1). The scenario in which ν_3 is heavier is denoted as the normal mass hierarchy (NH), and otherwise, in which ν_3 is lighter, it is denoted as the inverted mass hierarchy (IH) [20], as shown in Figure 2.2. Because the ν_1 has the greatest component of the electron neutrino ν_e while ν_3 has the slightest component of ν_e, the normal hierarchy in a crude way resembles the mass ordering of the charged leptons. Thus, its nomenclature is normal. In contrast, the inverted hierarchy represents the opposite situation.

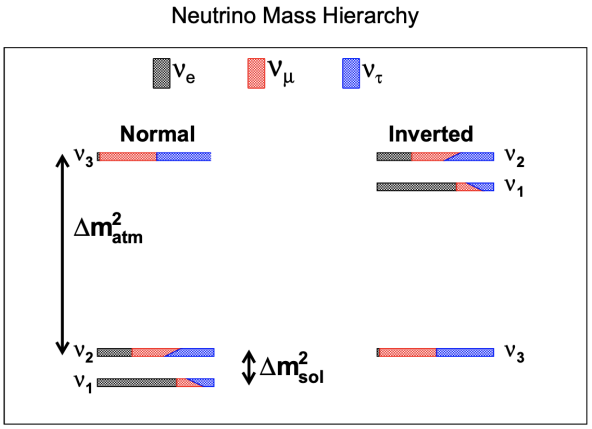

Figure 2.2: The diagram shows both the normal, left and inverted, right, mass hierarchy. It also shows the mass difference observed in atmospheric and solar experiments. In addition, it shows how each mass state is composed [20].

The neutrino flavours are each composed of 3 mass eigenstates, each with a different mass, m_i for $i = 1, 2, 3$. A superposition of these mass states is measured when a neutrino mass is measured. Therefore, the neutrino mass that is measured is an effective mass [20]. Figure 2.2 shows that each mass state can also be represented as a mixture of flavours. Neutrino mass experiments are trying to reveal the constraints on these three mass values to explain neutrino phenomena fully. Direct mass searches can find the effective neutrino mass to set rough constraints on light neutrino masses [17]. Conversely, in neutrinoless double beta decay, one could find the value of the lightest mass state or the effective electron neutrino mass upper limit.

2.2 The Dirac Neutrino Option

Neutrinos in the SM are described as Left-handed (LH) massless Wely fermions. As shown in section 2.1, the discovery of neutrino flavour oscillations implies non-zero neutrino masses. A simple way of explaining non-zero neutrino masses is to incorporate massless right-handed (RH) neutrinos into the SM that are singlet under the SM gauge group. In general, a fermion mass is included in the Lagrangian through the Dirac mass term [17],

$$m\overline{\psi}\psi. \tag{2.4}$$

If we take the field ψ and decompose it into left and right chiral states [17], ψ_L and ψ_R respectively, we can write (where $\overline{\psi_L}\psi_L = 0$ and $\overline{\psi_R}\psi_R = 0$)

$$m\overline{\psi}\psi = m\overline{\psi_L}\psi_R + m\overline{\psi_R}\psi_L. \tag{2.5}$$

As seen in equation 2.5, a non-zero mass term requires both left and right-handed chiral states. Moreover, the mass term can be regarded as a coupling constant between two chiral components [17]. With a neutral Higgs Boson, the Dirac mass term becomes neutrally charged and gauge invariant. The presence of RHNs allows a Yukawa term between LH and RH neutrinos and the SM Higgs doublet ϕ. Thus [10],

$$\mathcal{L}_N^D = \frac{i}{2}\overline{N}_I^R \not{\partial} N_I^R - y_{I\alpha}\overline{N}_I^R \tilde{\phi}^\dagger L_\alpha + h.c, \tag{2.6}$$

for $I = 1, 2, 3$ and $\alpha = e, \mu, \tau$. Here, $\tilde{\phi} = i\sigma_2\phi^*$ represents the hypercharge conjugated Higgs doublet, $y_{I\alpha}$ is a complex Yukawa coupling matrix, and $L_\alpha = (\nu_\alpha^L, \ell_\alpha^L)^T$ represents the SM LH, with flavor α, lepton doublet. Through equation 2.6, the neutrino mass generation is via the standard Higgs mechanism (HM). Through

electroweak symmetry breaking (EWSB) [10], the Higgs field acquires a non-zero vacuum expectation value (VEV), and massive Dirac fermions are formed through the combination of LH and RH neutrinos.

This case is denoted as the Dirac neutrino option. An appealing characteristic of this SM minimal extension is that it can implicitly explain BAU via neutrinogenesis [10]. The mechanism is based on the idea that the decay of heavy degrees of freedom (DOFs) in the early universe can lead to a primordial asymmetry between LH and RH neutrinos if RH neutrinos are included. Later, the sphaleron process converts the lepton number carried by the LH neutrinos L^L to baryon number B. However, the Dirac neutrino option cannot explain the tiny neutrino masses that experimental observation indicates. If a RH neutrino exists, it must not interact with other particles as it has not been observed. Thus, it is labelled as a "sterile" neutrino. Otherwise, there is another mechanism for mass generation, the Majorana mass mechanism.

2.3 The Majorana Neutrino Option

In early 1930, Ettore Majorana wondered if he could build a mass term with only a left-handed chiral state to omit the "sterile" right-handed neutrino state requirement [17]. He found that if we require the right-hand chiral state to be [17]

$$\psi_R = C\overline{\psi_L}^T. \tag{2.7}$$

Then we can write the field only in terms of ψ_L,

$$\psi = \psi_R + \psi_L = \psi_L + C\overline{\psi_L}^T = \psi_L + \psi_L^C, \tag{2.8}$$

where we have defined $\psi_L^C = C\overline{\psi_L}^T$. Equation 2.7 implies that the field and its charge conjugate are the same. Thus, a Majorana particle is its own antiparticle. The weak point of the Dirac neutrino option inspired the extension of equation 2.6 by an RH neutrino Majorana mass term [10],

$$\mathcal{L}_N^M = \frac{i}{2}\overline{N}_I^R \not{\partial} N_I^R - y_{I\alpha}\overline{N}_I^R \tilde{\phi}^\dagger L_\alpha - \frac{1}{2}\overline{N}_I^R M_{IJ}(N_J^R)^C + h.c. \tag{2.9}$$

Here, M_{IJ} can be selected to be real and diagonal, so $M_{IJ} = M_I\delta_{IJ}$. Upon EWSB equation 2.9, the SM neutrinos turn into Majorana fermions.

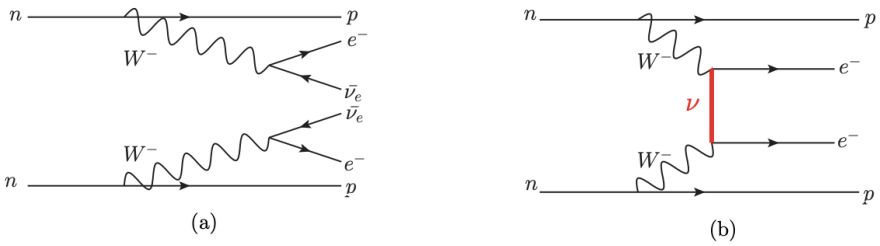

Figure 2.3: The first diagram (a) shows double beta decay with Dirac neutrinos. The second diagram (b) shows neutrinoless double beta decay with Majorana neutrinos [21].

If neutrinos are their own antiparticles, then it would lead to various implications. In ordinary double beta decay (Figure 2.3, a), through a weak interaction, two electron anti-neutrinos and two electrons are produced as two neutrons in a nucleus transform into protons [22],

$$(A, Z) \rightarrow (A, Z + 2) + 2e^- + 2\overline{v_e}. \tag{2.10}$$

However, neutrino-less double beta decay can occur if neutrinos are Majorana particles (Figure 2.3, b). The neutrino would be emitted and then absorbed in the same process [22],

$$(A, Z) \rightarrow (A, Z + 2) + 2e^-. \tag{2.11}$$

Thus, neutrino reactions would lead to lepton-violating phenomena since the lepton number is not conserved.

Chapter 3

Baryon Asymmetry

With the discovery of antiparticles and particle-antiparticle annihilation, the reason why our universe is mainly composed of matter has become an unresolved issue. Within human reach, the world and the rest of our solar system are mainly composed of ordinary matter. Further, antimatter is only found in accelerators or nuclear decays. Analysis of solar fluxes and fluxes of galaxies show us that most of the observable universe is composed of matter.

Studies concerning the universe's large-scale structure [23] and the cosmic microwave background CMB anisotropy from WMAP [24] grant us an approximate measure of the BAU. Measuring near the $e^{\pm}$ annihilation era, one compares the baryon number density to the photon density as their ratio is conserved provided that the B-violating reactions happen slowly (Both densities evolve inversely to a commoving volume R^{-3}),

$$\eta_B^{CMB} = \frac{\eta_B}{\eta_\gamma} = (6.1 \pm 0.2) \times 10^{-10}. \tag{3.1}$$

This ratio agrees with the computation from Big Bang Nucleosynthesis (BBN), where from astrophysical observations, the abundances of ^3He, ^4He, D, ^6Li, ^7Li are measured, which depend on the value of the baryon-to-photon ratio [25] [26],

$$\eta_B^{BBN} \approx (4.7 - 6.5) \times 10^{-10}. \tag{3.2}$$

Thus, the BBN result is consistent with the CMB result. As B-violating interactions are currently unknown, it is reasonable to assume that this asymmetry already existed in the early stages of the universe. Thermal quark-antiquark pairs were highly abundant in the primordial soup, and the maximal B-asymmetry at that

time was in the form of a small $q - \overline{q}$ asymmetry [27]:

$$\frac{n_q - n_{\overline{q}}}{n_q} \approx 3 \times 10^{-8}. \tag{3.3}$$

If the universe was created with such a small B-asymmetry, one could argue that an initially symmetric universe evolved to a slightly asymmetric one through leptogenesis.

3.1 The Sakharov Conditions

Sakharov laid down three essential features for a theory to produce the BAU, which is the following [28]: Baryon Number Violation, C and CP Violation, and interactions out of equilibrium. The nature of the mechanism for the BAU could differ, but all require these four components.

Baryon Number Violation is a requirement as without it, only a past asymmetry can cause a future asymmetry. GUT provides a framework where B and L violate interactions. However, the present SM lagrangian has no such interactions. Majorana neutrinos would violate the lepton number, which can then be transferred to baryon number by the sphaleron process.

C and CP Violation are shown to occur in the SM in insufficient amounts. C is maximally violated in the EW sector, and CP was violated in the Kaons decays. Since it is linked to SSB, one can expect to see it in all theory sectors. This is needed as the branching fractions for a particle, and its antiparticle must differ to obtain a higher amount of baryons than antibaryons.

if V baryons decay into two channels with branching rations f and $1-f$ and baryon number B_1 and B_2. In contrast $\overline{V}$ decay with different branching ratios a and $1-a$ into channels $-B_1$ and $-B_2$. The baryon number average generated by the decays of V and $\overline{V}$ is [27],

$$\begin{aligned}\Delta B &= \Delta B(V) + \Delta B(\overline{V}) \\ &= B_1|M(V \to B_1)| + B_2|M(V \to B_2)|^2 - B_1|M(\overline{X} \to B_1)| - B_2|M(\overline{V} \to B_2)|^2 \\ &= \frac{1}{2}(f-a)(B_1 - B_2).\end{aligned} \tag{3.4}$$

then $B_1 \neq B_2$ and C and CP ($f \neq a$) must be violated to have an asymmetry.

Out of equilibrium interactions must occur for a particle species to leave a relic, such as a neutrino decoupling and the decoupling of the CMB. For a baryon b and antibaryon $\overline{b}$, the density is proportional to [27],

$$n_b \propto \int_0^\infty \frac{1}{e^{(\sqrt{p^2+m_b^2}-\mu)/T}+1}\, dp, \tag{3.5}$$

$$n_{\overline{b}} \propto \int_0^\infty \frac{1}{e^{(\sqrt{p^2+m_{\overline{b}}^2}-\mu)/T}}\, dp \tag{3.6}$$

The entropy, in chemical equilibrium, reaches its maximum for vanishing chemical potentials (for all nonconserved quantum numbers). Further, in gauge theories, CPT invariance implies that both the particle and its antiparticle must have equal mass. Therefore, $n_b = n_{\overline{b}}$ in equilibrium, the process cannot happen.

3.2 Recipe for Leptogenesis

The Leptogenesis mechanism relates the BAU to the neutrino properties of the SM and their extensions, i.e. Seesaw Models and Supersymmetry. The process can be summarized as follows [29]: First, there must be a leptonic number-violating process, such as an RH Majorana particle decaying before EWPT. Thus, one violates the symmetry $B - L$. Then, the lepton asymmetry is almost washed out. One must solve the Boltzmann equation using the relevant particles' decay and inverse decay processes. Then, the remaining lepton asymmetry will convert to baryonic asymmetry due to the sphaleron effect.

A sphaleron is a static solution to the EW field equations in the SM. The sphaleron geometrically is a saddle point of the EW potential [30]; this point rests at the top of a barrier between two low-energy equilibria, labelled by two different baryon numbers. e.g. one equilibrium can consist of three baryons and the other of three antileptons in a system. One can tunnel through the barrier through an instanton-like process, and the system can convert between the two equilibria. e.g. from three baryons into three antileptons violating baryon and lepton numbers but conserving the difference. Hence converting the lepton asymmetry into baryonic asymmetry in leptogenesis.

Chapter 4

Type I Seesaw Mechanism

The Type I Seesaw model is given in equation 2.9. In Chapter 4, I will limit to a minimal Type I Seesaw Lagrangian incorporating only 2 RHN, N_I^R (I = 1, 2) for simplicity. In the 2 RHN seesaw model [10], $y_{I\alpha}$ in equation 2.9 is a rank-2 Yukawa matrix. This setup is enough to explain, in the SM neutrino sector, the two known nonzero mass-squared differences. In this case, one of the three SM neutrino masses, m_i (i = 1,2,3), will vanish, $\min(m_1, m_2, m_3) = 0$. Further, in resonant leptogenesis, the existence of a third RH neutrino is not necessary. It only needs two nearly degenerate RHN mass eigenstates. Since it is not required, it leaves room to add a third RHN that would not have a big effect on low-energy neutrino observables.

In Electroweak Symmetry Breaking (EWSB), the SM Higgs doublet archives a nonzero VEV, $\sqrt{2}\langle\phi_0\rangle = v \simeq 246$ GeV, which produces a matrix of complex Dirac masses, $(m_D)_{I\alpha}$, for LH and RH neutrinos. So [10],

$$\xrightarrow{\text{EWSB}} \frac{i}{2}\overline{N}_I^R \not{\partial} N_I^R - [(m_D)_{I\alpha} + y_{I\alpha}\phi_0]\overline{N}_I^R \nu_\alpha^L + y_{I\alpha}\phi_+ \overline{N}_I^R \ell_\alpha^L - \frac{1}{2}\overline{N}_I^R M_{IJ}(N_I^R)^C, \quad (4.1)$$

including its hermitian conjugate. Here ϕ_0 contains the real SM Higgs boson with a mass of $m_h \simeq 125$ GeV after EWSB. Further, the Dirac matrix is proportional to the RHN Yukawa matrix $(m_D)_{I\alpha} = y_{I\alpha}v/\sqrt{2}$. Organizing the Dirac and Majorana mass terms as follows [10],

$$\mathcal{L}_N^M \supset -\frac{1}{2}(\overline{(\nu_\alpha^L)^C}\ \overline{N_I^R}) \begin{pmatrix} 0_{\alpha\beta} & (m_D^T)_{\alpha J} \\ (m_D)_{I\beta} & M_{IJ} \end{pmatrix} \begin{pmatrix} \nu_\beta^L \\ (N_J^R)^C \end{pmatrix} + h.c, \quad (4.2)$$

one can identify the total neutrino mass matrix, $\mathcal{M}$, to conform to a 5×5 complex symmetric matrix. By Autonne-Takagi factorization, one can diagonalize $\mathcal{M}$ through a unitary matrix [10],

$$\mathcal{M}_{(\alpha,I)(\beta,J)} = \begin{pmatrix} 0_{\alpha\beta} & (m_D^T)_{\alpha J} \\ (m_D)_{I\beta} & M_{IJ} \end{pmatrix} \rightarrow \mathcal{D}_{(i,I)(j,J)} = \begin{pmatrix} D^v_{ij} & 0_{iJ} \\ 0_{Ij} & D^N_{IJ} \end{pmatrix}, \tag{4.3}$$

where D^v and D^N contain three light and two heavy Majorana mass eigenvalues, respectively, i.e. [10]

$$D^v_{ij} = m_i\delta_{ij}, \;\; D^N_{IJ} = M^{'}_I\delta_{IJ}. \tag{4.4}$$

The equations allow us to define $0 < M^{'}_1 \leq M^{'}_2$ without losing generality. However, in the case of light neutrinos, one must distinguish between the NH, $0 = m_1 < m_2 < m_3$, or the IH, $0 = m_3 < m_1 < m_2$. The ordering then determines the $\Delta m^2_{3\ell}$ sign. For NH, $\Delta m^2_{31} > 0$ and for IH, $\Delta m^2_{32} < 0$.

Now, one can switch to the seesaw limit, where the RH neutrino masses in equation 2.9 are greater than the Electroweak (EW) scale. In this scenario, RHNs decouple at high energies; Thus, there is no significant mixing at low energies between the sterile and active states. In this limit, one can approximately block diagonalize the total mass matrix [10],

$$\mathcal{M}_{(\alpha,I)(\beta,J)} \approx \begin{pmatrix} m_{\alpha\beta} & 0_{\alpha J} \\ 0_{I\beta} & M_{IJ} \end{pmatrix} \tag{4.5}$$

where a perturbative expansion, retaining the leading order (LO) terms, in the ratios of the form $(m_D)_{I\alpha}/M_{JK}$ was done. As shown, the RHN mass matrix in equation 2.9 coincides with the mass matrix for the heavy Majorana neutrinos in 4.5. The heavy neutrino mass eigenvalues correspond to the RHN input masses in the seesaw limit, i.e. $M_{IJ} = M_I\delta_{IJ} = D^N_{IJ} = M^{'}_I\delta_{IJ}$. For the light SM neutrino's Majorana masses, one obtains the following expression [10],

$$m_{\alpha\beta} = -(m_D^T)_{\alpha I}M^{-1}_{IJ}(m_D)_{J\beta}. \tag{4.6}$$

The expression 4.6 shows the Type I Seesaw suppresses the masses of light neutrinos with small Yukawa couplings and large masses for the RHN.

$m_{\alpha\beta}$ in equation 4.6 is a complex symmetric matrix, which can again be diagonalized by a unitary matrix U by Autonne-Takagi factorization [10],

$$(U^T)_{i\alpha}m_{\alpha\beta}U_{\beta j} = D^v_{ij} = m_i\delta_{ij}. \tag{4.7}$$

The U matrix associates the light neutrino mass eigenstates ν_i to the light neutrino flavour eigenstates ν^L_α by

$$\nu^L_\alpha = U_{\alpha i}\nu_i, \;\; \nu_i = (U^\dagger)_{i\alpha}\nu^L_\alpha = U^*_{\alpha i}\nu^L_\alpha. \tag{4.8}$$

One can carry out a unitary flavour transformation on the LH lepton doublet, L_α, as well as on the RH charged singlet ℓ^R_α before EWSB. Therefore, one assumes a diagonal mass matrix for the lepton flavours e, μ, τ. The charged lepton mass matrix leads to no contribution to lepton mixing. Hence, U can be identified as the Pontecorvo-Maki-Nakagawa-Sakata (PMNS) lepton mixing matrix, $U_{PMNS} = U$. U_{PMNS} is defined in the 2 RHN model as [31] [32],

$$U = \begin{pmatrix} c_{12}c_{13} & s_{12}c_{13} & s_{13}e^{-i\delta} \\ -s_{12}c_{23} - c_{12}s_{13}s_{23}e^{i\delta} & c_{12}c_{23} - s_{12}s_{13}s_{23}e^{i\delta} & s_{23}c_{13} \\ s_{12}s_{23} - c_{12}s_{13}c_{23}e^{i\delta} & -c_{12}s_{23} - s_{12}s_{13}c_{23}e^{i\delta} & c_{23}c_{13} \end{pmatrix} \begin{pmatrix} 1 & 0 & 0 \\ 0 & e^{i\sigma} & 0 \\ 0 & 0 & 1 \end{pmatrix} \quad (4.9)$$

where s_{ij} and c_{ij} are shorthand notation for $\sin\theta_{ij}$ and $\cos\theta_{ij}$, respectively. Further, the PMNS mixing angles are $\theta_{12}, \theta_{23}, \theta_{13} \in [0, \pi/2)$, $\delta \in [0, 2\pi)$ is the CP violating phase, and $\sigma \in [0, \pi)$ is the CP violating Majorana phase in the 2 RHN seesaw. The second Majorana phase in the 3 RHN model, τ, can be rotated away by a phase transformation on the massless neutrino mass eigenstate. The current list of experimental constraints attained from global fit analysis is shown in Table 4.1. However, no current experimental constraint exists for the σ phase.

Table 4.1: Neutrino Experimental Constraints [33] [34] [35]

Parameter	Normal Hierarchy		Inverted Hierarchy	
	Best fit Value	3σ	Best fit Value	3σ
$\Delta m^2_{21}/10^{-5}$	7.39	6.79 – 8.01	7.39	6.79 – 8.01
$\Delta m^2_{21}/10^{-5}$	2.525	2.431 – 2.622	2.512	2.413 – 2.606
$sin^2\theta_{12}$	0.310	0.275 – 0.350	0.310	0.275 – 0.350
$sin^2\theta_{23}$	0.582	0.428 – 0.624	0.582	0.433 – 0.623
$sin^2\theta_{13}$	0.02240	0.02044 – 0.02437	0.02263	0.02067 – 0.02461
δ	3.79	2.36 – 6.39	4.89	3.42 – 6.13
σ	-	$0 - \pi$	–	$0 - \pi$

From the expression 4.6 and 4.12, one can obtain the following expression [10],

$$(U^T)_{i\alpha} m_{\alpha\beta} U_{\beta j} = -[M_I^{-1/2}(m_D)_{I\alpha} U_{\alpha i}]^T \delta_{IJ} [M_j^{-1/2}(m_D)_{J\beta} U_{\beta j}] = m_i \delta_{ij}. \quad (4.10)$$

This can be used to solve for $(m_D)_{I\alpha}$, or equivalently for Yukawa matrix $y_{I\alpha}$ [10],

$$y_{I\alpha} = \frac{(m_D)_{I\alpha}}{v/\sqrt{2}} = \frac{i}{v/\sqrt{2}} M_I^{1/2} R_{Ii} m_i^{1/2} (U^\dagger)_{i\alpha}, \quad (4.11)$$

where the matrix R is a complex rotation matrix that follows $RR^T = I_{2\times 2}$. Expression 4.11 is known as the Casas-Ibarra parametrization (CIP) of the RH neutrino

Yukawa matrix [36]. The R matrix can be further parametrized by a discrete parameter $\zeta = \pm 1$ and a complex rotation angle z. Here, ζ distinguishes between the positive and negative branches of possible R matrices. Then [10],

$$NH : R(z)_\zeta = \begin{pmatrix} 0 & \cos(z) & \zeta \sin(z) \\ 0 & -\sin(z) & \zeta \cos(z) \end{pmatrix}, \quad IH : R(z)_\zeta = \begin{pmatrix} \cos(z) & \zeta \sin(z) & 0 \\ -\sin(z) & \zeta \cos(z) & 0 \end{pmatrix}, \tag{4.12}$$

where $z = z_R + i z_I$ has two DOFs, it reflects the model's mismatch between high and low energy parameters.

4.1 Heavy right-handed neutrino Leptogenesis

Leptogenesis relates the BAU to the properties of neutrinos. Here, decays of heavy Majorana neutrinos generate a lepton asymmetry, which is then partially transformed through a sphaleron process to a baryon asymmetry. We now focus on a single flavour regime of leptogenesis, a model based on the decay of the lightest heavy RH neutrino, for simplicity to illustrate the ideas the theory entails.

The model, which was first proposed by Fukugita and Yanagida, uses a Type I Seesaw Mechanism for neutrino mass generation [37]. In the model, RH heavy neutrinos ($SU(5)$ Sterile) are described by Yukawa couplings with Higgs and leptons [38]. In the universe's early stages, RH heavy neutrinos (due to their heaviness) quickly decouple from the primordial thermal bath and decay into scalar bosons, leptons and antileptons. Then, the surplus of leptons over anti-leptons at this time is determined by the strength of CP violation in the lepton sector. Here, for simplicity, we assume the RH heavy neutrinos have a mass Hierarchy $M_1 < M_2 < M_3$. Thus, the later decay of N_1 (lightest one) will wash out the lepton number generated by N_2, N_3. Provided that the interactions that follow are CP-conserving, when the decay reaction freezes out, the lepton asymmetry will evolve without being affected. Then, the lepton asymmetry is converted to baryon asymmetry (Sphaleron Process) by non-perturbative $B + L$ violating processes that are in equilibrium.

Starting with the Lagrangian with a Type I Seesaw with m ($m \geq 2$) singlet RH neutrinos N_{Ri} [38],

$$\mathcal{L} \supset i\overline{N}_{Ri} \not{\partial} N_{Ri} - \frac{1}{2} M_i \overline{N_{Ri}^C} N_{Ri} - \epsilon_{ab} Y_{\alpha i} \overline{N_{Ri}} \ell_\alpha^a H^b - h.c. \tag{4.13}$$

where M_i are the Majorana masses of the RH neutrino, $\ell_\alpha = (\nu_{\alpha L}, \alpha_L^-)$ with $\alpha = e, \mu, \tau$ are the LH lepton doublet and $H = (H^+, H^0)$ is the Higgs doublet. Further,

$\epsilon_{ab} = -\epsilon_{ba}$ with $\epsilon_{12} = 1$. This difference is induced if CP is violated through 1-loop corrections by a Higgs particle. The net lepton number production due to the decay of N_{R1} arises from the interference of diagrams in Figure 4.1.

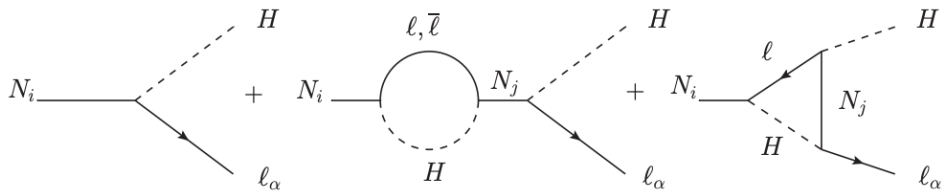

Figure 4.1: The CP asymmetry in the Type I seesaw model comes from the interference among the one-loop wave and vertex diagrams. For the one-loop diagram, there is an extra L-conserving diagram contributing to the CP asymmetry (this vanishes when summing lepton flavours) [38].

The CP asymmetry in the decays of N_i can be defined as [38]

$$\epsilon_{i\alpha} = \frac{|A_0(N_i \to \ell_\alpha H)|^2 - |A_0(N_i \to \overline{\ell_\alpha} H^*)|^2}{\sum_\alpha |A_0(N_i \to \ell_\alpha H)|^2 - |A_0(N_i \to \overline{\ell_\alpha} H^*)|^2} \tag{4.14}$$

where $A_0(i \to f)$ denotes the decay amplitude at zero temperature. The equation 4.14 vanishes as tree level, but at 1-loop, there's interference between the self-energy, wave diagram, and vertex diagram [37] [39]. At leading order we obtain [38],

$$\begin{aligned} \epsilon_{i\alpha} =& \frac{1}{8\pi} \frac{1}{(Y^\dagger Y)_{ii}} \sum_{j \neq i} Im[(Y^\dagger Y)_{ji} Y_{\alpha i} Y^*_{\alpha j})] g(\frac{M_j^2}{M_i^2}) \\ &+ \frac{1}{8\pi} \frac{1}{(Y^\dagger Y)_{ii}} \sum_{j \neq i} Im[(Y^\dagger Y)_{ij} Y_{\alpha i} Y^*_{\alpha j})] \frac{M_i^2}{M_i^2 - M_j^2}. \end{aligned} \tag{4.15}$$

where the loop function is

$$g(x) = \sqrt{x}\Big[\frac{1}{1-x} + 1 - (1+x)\ln(\frac{1+x}{x})\Big] \tag{4.16}$$

The first term in equation 4.15 consists of vertex and L-violating wave diagrams. The second term consists of the L-conserving wave diagram, which, if $M_i \approx M_j$, can resonantly enhance the CP asymmetry. In the one flavour regime, summing over the index α leads to [38],

$$\epsilon_i = \sum_\alpha \epsilon_{i\alpha} = \frac{1}{8\pi} \frac{1}{(Y^\dagger Y)_{ii}} \sum_{j \neq i} Im[(Y^\dagger Y)^2_{ji}] g(\frac{M_j^2}{M_i^2}). \tag{4.17}$$

Because the combination of Yukawa couplings is real, the second term in equation 4.15 vanishes. Defining abundances as the ratio of particle density (n_i) to entropy density (s), $Y_i = n_i/s$. Then, when the mass of the heavy RH neutrino is more than the temperature of the universe, the RHN decouple from the thermal bath, generating a lepton asymmetry [38],

$$Y_L = \epsilon_1 \eta_1 Y_{N_1}, \tag{4.18}$$

where η_1 is the efficiency factor (separating weak and strong washout regimes) and Y_{N_1} is a solution to a Boltzmann equation as in reference [38]. If leptogenesis ends before the EW sphaleron process becomes active, the $B - L$ asymmetry Y_{B-L} is

$$Y_{B-L} = -Y_L. \tag{4.19}$$

Then, the $B - L$ asymmetry is partly converted to a B asymmetry through the sphaleron process, [40]

$$Y_B = \frac{28}{79} Y_{B-L}. \tag{4.20}$$

This equation holds if sphalerons decouple before EWPT. Hence, besides giving an explanation of the light neutrino masses, the three Sakharov's conditions for leptogenesis are met. Here, Lepton number violation (LNV) is provided by the Majorana nature, the complexity of the Yukawa coupling ensures CP violation and the requirement that the N_i decay rate is not as quick as the Hubble expansion rate at $T = M_i$ guarantees the departure from thermal equilibrium.

Chapter 5

Type II Seesaw Mechanism

In the Type II Seesaw mechanism [11], the SM scalar sector is minimally extended by a $SU(2)_L$ triplet scalar Δ, which carries a hypercharge of 1. The addition of this new field results in a natural framework explaining the neutrino masses' smallness. The triplet and SM doublet Higgs's in this model are parameterized as [11],

$$H = \begin{pmatrix} h^+ \\ h \end{pmatrix}, \quad \Delta = \begin{pmatrix} \Delta^+/\sqrt{2} & \Delta^{++} \\ \Delta^0 & -\Delta^+/\sqrt{2} \end{pmatrix} \tag{5.1}$$

where h and Δ^0 are the neutral components of H and Δ, respectively. Further, the charged components of the triplet Higgs, Δ^+ and Δ^{++}, have a significant role in collider experiments and are integral to discovering a Type II Seesaw.

Adding a triplet Higgs will lead to new interactions involving the LH lepton doublet and the SM Higgs. Particularly, there is a new Yukawa interaction between the LH Lepton doublet L_i and the triple scalar Δ [11],

$$\mathcal{L}_{Yukawa} = \mathcal{L}^{SM}_{Yukawa} - \frac{1}{2} y_{ij} \overline{L}_i^C \Delta L_j + h.c. \tag{5.2}$$

This Yukawa interaction is crucial in generating a nonzero neutrino mass matrix when the neutral component of Δ obtains a nonzero VEV. In addition, this interaction attributes to the triplet Higgs a lepton charge of $Q_L = -2$ (satisfying one of the requirements of the Affleck-Dine mechanism). Including Δ prompts new terms in the Higgs' potential $V(H, \Delta)$, containing interactions related to the triplet scalar

that cause global LNV. This potential is [11],

$$\begin{aligned} V(H,\Delta) = &- m_H^2 H^\dagger H + \lambda_H (H^\dagger H)^2 + m_\Delta^2 Tr(\Delta^\dagger \Delta) + \lambda_1 (H^\dagger H) Tr(\Delta^\dagger \Delta) + \\ &\lambda_2 (Tr(\Delta^\dagger \Delta))^2 + \lambda_3 Tr(\Delta^\dagger \Delta)^2 + \lambda_4 H^\dagger \Delta \Delta^\dagger H + \Big[\mu (H^T i\sigma^2 \Delta^\dagger H) \\ &+ \frac{\lambda_5}{M_p} (H^T i\sigma^2 \Delta^\dagger H)(H^\dagger H) + \frac{\lambda_5^{'}}{M_p} (H^T i\sigma^2 \Delta^\dagger H)(\Delta^\dagger \Delta) + h.c \Big] + \dots \end{aligned} \tag{5.3}$$

where the terms in brackets cause LNV and the μ dependant cubic term are used to determine the VEV of Δ^0. In addition, the five dimension operators suppressed by M_p have been included (Plank Scale). In low-energy physics, they play no role. However, they can become important during the inflation and reheating of early universe epochs.

Focusing on the neutral components of Δ and H with non-trivial VEVs, the potential can be simplified as [11],

$$\begin{aligned} V(h,\Delta^0) = &- m_H^2 |h|^2 + \lambda_H |h|^4 + m_\Delta^2 |\Delta^0|^2 + \lambda_\Delta |\Delta^0|^4 + \lambda_{H\Delta} |h|^2 |\Delta^0|^2 \\ &- \Big(\mu h^2 \Delta^{0*} + \frac{\lambda_5}{M_p} |h|^2 h^2 \Delta^{0*} + \frac{\lambda_5^{'}}{M_p} |\Delta^0|^2 h^2 \Delta^{0*} + h.c \Big) + \dots \end{aligned} \tag{5.4}$$

Here $\lambda_\Delta = \lambda_2 + \lambda_3$ and $\lambda_{H\Delta} = \lambda_1 + \lambda_4$. Notice that these parameters must carry values which satisfy the vacuum stability conditions and require both h and Δ^0 to have nonzero VEVs in the early universe to ensure the breaking of the $U(1)_L$ term.

From the potential in equation 5.4, one can derive the VEV of Δ. In the limit, $m_\Delta \ll v_{EW}$, where the SM Higgs VEV is substantially smaller than the triplet Higgs mass parameter, one finds the triplet Higgs non-vanishing VEV to be [11],

$$v_\Delta = \langle \Delta^0 \rangle \simeq \frac{\mu v_{EW}^2}{2 m_\Delta^2}, \tag{5.5}$$

where the SM Higgs VEV is $v_{EW} = 246$ GeV. Further, a lower limit, $m_\Delta \gtrsim 800$ GeV, has been placed from searches on the doubly-charged Higgs in the LHC [41]. The charged and neutral components of Δ have masses approximately $m_{\Delta^{++}} \simeq m_{\Delta^+} \simeq m_{\Delta^0} \simeq m_\Delta$ in the $m_\Delta > 800$ GeV range.

The Yukawa interaction in equation 5.4, generates the following mass matrix of the neutrinos [11],

$$m_{ij}^v = y_{ij} v_\Delta. \tag{5.6}$$

Then, by a similar method to Type I Seesaw, one can diagonalize the matrix in

equation 5.2 by the PMNS matrix. To guarantee that the neutrino Yukawa couplings remains perturbative up to the Plank scale, y_v has to be smaller than $\mathcal{O}(1)$. The VEV of Δ^0 is now given by the following range [11],

$$\mathcal{O}(1)\,\text{GeV} > |\langle\Delta^0\rangle| \gtrsim 0.05\,\text{eV}. \tag{5.7}$$

The upper bound on Δ^0 VEV is derived from the T-parameter constraints in precision measurements [42] and the lower limit ensures the generation of the small neutrino masses (Also allows perturbative Yukawa couplings). If the Type II seesaw model is responsible for inflation, it can generate the BAU during inflation through the Affleck-Dine mechanism. However, it requires a non-minimal coupling amidst the Higgs and the Ricci scalar.

5.1 Afflect-Dine Mechansim Leptogenesis

Following the inflationary setup and inflationary trajectory from reference [11], the authors also extended the SM lagrangian by adding a term for a non-minimal coupling of the triple Higgs with gravity. Here, combining the scalar sector with the non-minimal coupling leads to [11] (with Ricci scalar R),

$$\begin{aligned}\frac{\mathcal{L}}{\sqrt{-g}} = &-\frac{1}{2}M_p^2 R - F(H,\Delta)R - g^{\mu\nu}(D_\mu H)^\dagger(D_\nu H) \\ &- g^{\mu\nu}(D_\mu\Delta)^\dagger(D_\nu\Delta) - V(H,\Delta) + \mathcal{L}_{Yukawa},\end{aligned} \tag{5.8}$$

where the non-minimal couplings take the form [11],

$$F(H,\Delta) = \xi_H|h|^2 + \xi_\Delta|\Delta^0|^2 = \frac{1}{2}\xi_H\rho_H^2 + \frac{1}{2}\xi_\Delta\rho_\Delta^2. \tag{5.9}$$

Here, we have introduced

$$h = \frac{1}{\sqrt{2}}\rho_H e^{i\eta}, \quad \Delta^0 = \frac{1}{\sqrt{2}}\rho_\Delta e^{i\theta}. \tag{5.10}$$

Now, by defining the inflation as φ through the following relations [11],

$$\rho_H = \varphi\sin\alpha, \;\; \rho_\Delta = \varphi\cos\alpha, \;\; \xi = \xi_H\sin^2\alpha + \xi_\Delta\cos^2\alpha, \tag{5.11}$$

the Lagrangian simplifies to

$$\frac{\mathcal{L}}{\sqrt{-g}} = -\frac{M_p^2}{2}R - \frac{\xi}{2}\varphi^2 R - \frac{1}{2}g^{\mu\nu}\partial_\mu\varphi\partial_\nu\varphi - \frac{1}{2}\varphi^2\cos^2\alpha\, g^{\mu\nu}\partial_\mu\theta\partial_\nu\theta - V(\varphi,\theta). \tag{5.12}$$

where,

$$V(\varphi,\theta)=\frac{1}{2}m^2\varphi^2+\frac{\lambda}{4}\varphi^4+2\varphi^3\Big(\tilde{\mu}+\frac{\tilde{\lambda_5}}{M_p}\varphi^2\Big)\cos\theta. \tag{5.13}$$

and

$$\begin{aligned}
m^2&=m_\Delta^2\cos^2\alpha-m_H^2\sin^2\alpha,\\
\lambda&=\lambda_H\sin^4\alpha+\lambda_{H\Delta}\sin^2\alpha\cos^2\alpha+\lambda_\Delta\cos^4\alpha,\\
\tilde{\mu}&=-\frac{1}{2\sqrt{2}}\mu\sin^2\alpha\cos\alpha,\\
\tilde{\lambda_5}&=-\frac{1}{4\sqrt{2}}(\lambda_5\sin^4\alpha\cos\alpha+\lambda_5^{'}\sin^2\alpha\cos^3\alpha).
\end{aligned} \tag{5.14}$$

The Afflect-Dine (AD) mechanism will be realised through the dynamical field θ. The motion provoked in θ by inflation sets the size of the lepton asymmetry. The quartic term in the potential dominates as $m \ll \varphi$ during inflation. Now, changing from the Jordan frame to the Einstein frame through the transformation [11]

$$g^{\mu\nu}=\Omega^2 g_{\mu\nu},\ \tilde{\Omega^2}=1+\xi\frac{\varphi^2}{M_p^2} \tag{5.15}$$

and reparamtrizing in terms of a canonically nomarlized scalar χ. Changing from the Jordan frame to the Einstien frame, φ no longer has a canonically normalized kinetic term. So, the following field redefinition is required [11],

$$\frac{d\chi}{d\varphi}=\frac{\sqrt{(6\xi^2\varphi^2/M_p^2+\Omega^2)}}{\Omega^2}. \tag{5.16}$$

This then gives χ in terms of φ as

$$\chi=\frac{1}{\sqrt{\xi}}\Big(\sqrt{1+6\xi}\sinh^{-1}(\sqrt{\xi+6\xi^2}\varphi)-\sqrt{6\xi}\sinh^{-1}(\sqrt{6\xi^2}\varphi/\sqrt{1+\xi\varphi^2})\Big) \tag{5.17}$$

. Thus, we now obtain the final Einstein frame Lagrangian [11],

$$\frac{\mathcal{L}}{\sqrt{-g}}=-\frac{M_p^2}{2}R-\frac{1}{2}g^{\mu\nu}\partial_\mu\chi\partial_\nu\chi-\frac{1}{2}f(\chi)g^{\mu\nu}\partial_\mu\theta\partial_\nu\theta-U(\chi,\theta), \tag{5.18}$$

where

$$f(\chi)=\frac{\varphi(\chi)^2\cos^2\alpha}{\Omega^2(\chi)},\ U(\chi,\theta)=\frac{V(\varphi(\chi),\theta)}{\Omega^4(\chi)}. \tag{5.19}$$

The core idea behind the AD mechanism [43] is the generation of nonzero angular motion in the phase of ϕ, a complex scalar field charged with a global $U(1)$ symmetry. If, in the universe's early stages, ϕ gains a large initial field value, ϕ will

oscillate once the Hubble parameter decreases below the mass m of ϕ. If the potential of the scalar incorporates a $U(1)$ breaking term, the motion will generate a $U(1)$ charge asymmetry. Consequently, if the symmetry consists of $U(1)_B$ or $U(1)_L$ symmetries, a baryon asymmetry will be acquired before EWPT. In this case, φ can be ϕ (The global $U(1)_L$ symmetry is carried by the complex phase of the mixed state of the SM and triplet Higgs).

Identifying ϕ with the scalar for inflation and the complex phase of the triplet Higgs, the asymmetry number density associated with the $U(1)_L$ charge is [11],

$$n_L = Q_L \varphi^2(\chi) \dot{\theta} \cos^2 \alpha, \tag{5.20}$$

where α is the mixing angle between the SM and triplet Higgs during inflation. To acquire a nonzero n_L, lepton asymmetry density, one needs a non-trivial motion in phase θ and a nonzero VEV for χ. The net lepton asymmetry will then be converted to a baryon asymmetry through the sphaleron process.

The equations of motion for χ and θ can be derived as,

$$\ddot{\chi} - \frac{1}{2} f_{,\chi} \dot{\theta}^2 + 3H\dot{\chi} + U_{,\chi} = 0, \tag{5.21}$$

$$\ddot{\theta} + \frac{f_{,\chi}}{f(\chi)} \dot{\theta}\dot{\chi} + 3H\dot{\theta} + \frac{1}{f(\chi)} U_{,\theta} = 0. \tag{5.22}$$

Evaluating equations 5.21 and 5.22 in the inflationary epoch, one finds the slow-roll regimes [11],

$$\dot{\chi} \simeq -\frac{M_p U_{,\chi}}{\sqrt{3U}}, \;\; \dot{\theta} \simeq -\frac{M_p U_{,\theta}}{f(\chi)\sqrt{3U}} \tag{5.23}$$

During inflation, since χ approaches M_p one can ignore the m and $\tilde{\mu}$ terms in the potential, which are less than M_p. Using these approximations, the asymmetry generated by the triplet Higgs phase θ at the end of inflation is [11],

$$\begin{aligned} n_{Lend} &= Q_L \varphi_{end}^2 \dot{\theta}_{end} \cos^2 \alpha \\ &\simeq -\mathcal{O}(1) Q_L \varphi_{end}^2 \frac{M_p U_{,\theta}}{f(\chi_{end})\sqrt{3U_{end}}} \cos^2 \alpha \\ &\simeq -\mathcal{O}(1) Q_L \tilde{\lambda_5} \varphi_{end}^3 \sin\theta_{end} / \sqrt{3\lambda}. \end{aligned} \tag{5.24}$$

Here, the $\mathcal{O}(1)$ factor comes from numerical calculations in reference [11]. It accounts for the breakdown of the slow-roll approximation at the end of inflation, and it is roughly three. The last step consists of assuming that the quartic term in the potential is dominant and that LNV interactions are dominated by $\tilde{\lambda_5}$ coupling.

The produced nonzero lepton number density n_L will come as neutrinos once reheating is finished. Then, the lepton number will be redistributed into baryons through an EW sphaleron process by the following relation [40],

$$n_B \simeq -\frac{28}{79} n_L. \tag{5.25}$$

As in reference [11], for the reheating process at $t_{reh} = 223/H_0$ and Hubble parameter $H_{reh} = 0.0047 H_0$. The relation $H_{reh}^2 \simeq (\pi^2/90) g_* (T_{ref}^4/M_p^2)$ gives $T_{ref} \approx 2.2 \times 10^{14}$ GeV. Then considering the entropy density $s = (2\pi^2/45) g_* T_{reh}^3$ then the authors obtained [11],

$$\eta_B = \frac{n_B}{s} = \eta_B^{obs} \Big(\frac{|n_{Lend}|/M_p^3}{1.3 \times 10^{-16}} \Big) \Big(\frac{g_*}{112.75} \Big)^{-1/4} \tag{5.26}$$

where η_B^{obs} is the parameter for the observed baryon asymmetry, and g_* is the DOF at the present time of reheating.

This expression reveals that at the end of inflation, a lepton number asymmetry of the magnitude $1.3 \times 10^{-16} M_p^3$ is needed to produce the current baryon asymmetry. The corresponding parameters for this result (from numerical calculations) in this model are the following: $\tilde{\lambda_5} = 7 \times 10^{-15}$ for $\theta_0 = 0.1$ and $\tilde{\lambda_5} = 10^{-10}$ for $\theta_0 = 6.5 \times 10^{-6}$ [11]. Thus, these parameters illustrate the wide range of values for successful leptogenesis.

Chapter 6

Type III Seesaw Mechanism

In the Type III Seesaw Mechanism, one introduces a triplet lepton representing $\Sigma : (1, 3, 0)$ to generate the Seesaw neutrino mass matrix [12]. This model consists, besides the SM particles, of three LH triplets of leptons, which carry a Hypercharge of 0,

$$\Sigma = \begin{pmatrix} N^0/\sqrt{2} & E^+ \\ E^- & -N^0/\sqrt{2} \end{pmatrix}, \quad \Sigma^C = \begin{pmatrix} N^{0C}/\sqrt{2} & E^{-C} \\ E^{+C} & -N^{0C}/\sqrt{2} \end{pmatrix}. \tag{6.1}$$

The renormalizable Lagrangian related to Σ is [12],

$$\mathcal{L} = Tr[\overline{\Sigma} i D\Sigma] - \frac{1}{2} Tr[\overline{\Sigma} M_\Sigma \Sigma^C + \overline{\Sigma^C} M_\Sigma^* \Sigma] - \tilde{H}^\dagger \overline{\Sigma} \sqrt{2} Y_\Sigma L_L - \overline{L_L} \sqrt{2} Y_\Sigma^\dagger \Sigma \tilde{H} + h.c. \tag{6.2}$$

Defining $E = E_R^{+c} + E_R^-$, one obtains the Lagrangian,

$$\begin{aligned} \mathcal{L} = {} & \overline{E} i\partial\!\!\!/ E + \overline{N_R^0} i\partial\!\!\!/ N_R^0 - \overline{E} M_\Sigma E - \left(\overline{N_R^0} \frac{M_\Sigma}{2} N_R^{0C} + h.c. \right) \\ & + g\left(W_\mu^+ \overline{N_R^0} \gamma_\mu P_R E + W_\mu^+ \overline{N_R^{0C}} \gamma_\mu P_L E + h.c. \right) - g W_\mu^3 \overline{E} \gamma_\mu E \\ & - \left(\phi^0 \overline{N_R^0} Y_\Sigma v_L + \sqrt{2} \phi^0 \overline{E} Y_\Sigma l_L + \phi^+ \overline{N_R^0} Y_\Sigma l_L - \sqrt{2} \phi^+ \overline{v_L^C} Y_\Sigma^T E + h.c \right). \end{aligned} \tag{6.3}$$

Then, one can identify the neutrino mass terms in equation 6.3 to obtain [12],

$$\mathcal{L} \supset -(\overline{v_L^C} \ \overline{N^0}) \begin{pmatrix} 0 & Y_\Sigma^T v/2\sqrt{2} \\ Y_\Sigma v/2\sqrt{2} & M_\Sigma/2 \end{pmatrix} \begin{pmatrix} v_L \\ N^{0C} \end{pmatrix} + h.c, \tag{6.4}$$

a standard seesaw matrix. The charged partners in the triplet Σ mix with the SM charged leptons, resulting in the following mass matrix,

$$\mathcal{L} \supset -(\overline{l_R} \ \overline{E_R}) \begin{pmatrix} m_l & 0 \\ Y_\Sigma v & M_\Sigma \end{pmatrix} \begin{pmatrix} l_L \\ E_L \end{pmatrix} + h.c. \tag{6.5}$$

After introducing unitary matrices as in the Type I Seesaw model, as in [10]. One can diagonalize the mass matrix and mass eigenvalues for the neutrinos and charged leptons [44],

$$diag(N) = U_0^\dagger \begin{pmatrix} 0 & Y_\Sigma^\dagger v/2\sqrt{2} \\ Y_\Sigma^* v/2\sqrt{2} & M_\Sigma^* \end{pmatrix} U_0^* = \begin{pmatrix} m_v^{diag} & 0 \\ 0 & M_N^{diag} \end{pmatrix}, \tag{6.6}$$

$$diag(E) = U_L^\dagger \begin{pmatrix} m_l^\dagger & Y_\Sigma^\dagger v_0 \\ 0 & M_\Sigma^\dagger \end{pmatrix} U_R = \begin{pmatrix} m_l^{diag} & 0 \\ 0 & M_E^{diag} \end{pmatrix}. \tag{6.7}$$

where the light neutrino mass eigenstates are denoted by v_j for $j = 1, 2, 3$. Here, the heavy neutral leptons are donated as N_j and the charged leptons as $E_k^\pm$. Explicitly in the expansion, the light and heavy neutrino mass eigenvalues are [44],

$$m_v \approx \frac{Y_\Sigma^2 v_0^2}{2M_\Sigma}, \;\; M_N \approx M_\Sigma \tag{6.8}$$

and for charged leptons are,

$$m_l - m_l \frac{Y_\Sigma^2 v_0^2}{2M_\Sigma} \approx m_l, \;\; M_E \approx M_\Sigma. \tag{6.9}$$

At the tree level, the heavy leptons N and $E^\pm$ are degenerate in mass. However, after EWSB, and for $M_\Sigma \geq 100$ GeV, radiative corrections split this degeneracy by [44],

$$\Delta M \equiv M_E - M_N = \frac{\alpha_W}{2\pi} \frac{M_W^2}{M_\Sigma} \Big[f\big(\frac{M_\Sigma}{M_Z}\big) - f\big(\frac{M_\Sigma}{M_W}\big) \Big] \approx 160\text{MeV} \tag{6.10}$$

where,

$$f(y) = \frac{1}{4y^2} \log(y^2) - (1 + \frac{1}{4y^2}) \sqrt{4y^2 - 1} \arctan(\sqrt{4y^2 - 1}). \tag{6.11}$$

This opens the $E_\pm \to N\pi^\pm$; after this, heavy lepton decays to electroweak bosons and light leptons that progress through double-triplet lepton mixing.

The heavy triplet leptons have gauge interactions compared to the Type I Seesaw. Thus, their detection is easier if, kinematically, these particles can be produced in colliders. Further, gauge interactions also contribute to the Leptogenesis processes. In the Type III Seesaw model, LNV is provided by the term, $-\frac{1}{2} Tr[\overline{\Sigma} M_\Sigma \Sigma^C + \overline{\Sigma^C} M_\Sigma^* \Sigma]$ in the Lagrangian, violating the lepton number by two units. The lepton number asymmetry is caused by N_0 and $E_i^\pm$ decays.

6.1 Heavy fermion Leptogenesis

Leptogenesis is the process where one transforms the LNV into a baryon number violation. The main idea behind the mechanism, apart from the Sakharov conditions, is that at a high enough temperature, the sphaleron effect can transfer lepton number asymmetry into the BAU. The sphaleron effect violates B and L but conserves $B - L$. When the effect occurs, $B - L$ is preserved, but $B + L$ is washed out. If the $B + L$ washout is finished, for an initial non-zero L_i, but zero B_i, after sphaleron effect, the final baryon number B_f and final lepton number L_f is [12],

$$B_i - L_i = B_f - L_f, \quad B_f + L_f = 0 \to B_f = -\frac{1}{2}L_i, \quad L_f = \frac{1}{2}L_i. \tag{6.12}$$

In an SM with a Higgs doublet, as shown previously, $B_f = -28/79 L_i$ (the washout is imperfect).

In the Type III seesaw model, the Majorana mass term for heavy neutrino N violates the lepton number. When N decays, it generates a lepton number asymmetry ϵ_N for a CP-violating interaction. If the process occurs out of equilibrium, a net lepton asymmetry can be created. Then, through the sphaleron effect, one would have, at present [12],

$$\frac{n_B}{n_\gamma} = -\frac{28}{79} Y_N^{eq} \epsilon_N \eta. \tag{6.13}$$

where $Y_N^{eq} = n^{eq}/s$ with n_N^{eq} is the density of N at equilibrium, s is the entropy density, and η is the efficiency factor of surviving washout. η is then determined by solving a Boltzmann equation considering the lepton number conversing (washout asymmetry) and conserving process, which is model-independent.

In the Type III model, the LNV is provided by the 2nd term in equation 6.2, which has a LNV of two units. Here, the decays of N^0 and $E_i^\pm$ produce a lepton number asymmetry. The lepton number asymmetry ϵ_1 by the lightest neutrino and charged partners is [12],

$$\epsilon_1 = -\sum_{j=2,3} \frac{3}{2} \frac{M_1}{M_j} \frac{\Gamma_j}{M_j} I_J \frac{2S_j - V_j}{3}, \tag{6.14}$$

where

$$I_j = \frac{Im[(\lambda\lambda^\dagger)_{1j}^2]}{|\lambda\lambda^\dagger|_{11}|\lambda\lambda^\dagger|_{jj}}, \tag{6.15}$$

$$\frac{\Gamma_j}{M_j} = \frac{|\lambda\lambda^\dagger|_{jj}}{8\pi} = \frac{\tilde{m}_j M_j}{8\pi v^2}, \tag{6.16}$$

$$S_j = \frac{M_j^2 \Delta M_{1j}^2}{(\Delta M_{1j}^2)^2 - M_1^2 \Gamma_j^2}, \tag{6.17}$$

$$V_j = 2\frac{M_j^2}{M_1^2}\left[(1+\frac{M_j^2}{M_1^2})\log(1+\frac{M_1^2}{M_j^2})-1\right] \tag{6.18}$$

where S_j and V_j are functions due to Feynman diagrams, and finally,

$$\Delta M_{ij}^2 = M_j^2 - M_i^2, \quad \lambda = Y_\Sigma/\sqrt{2}. \tag{6.19}$$

In the hierarchical limit ($M_{2,3} \ll M_1$) of the heavy leptons [12],

$$\epsilon_1 = \sum_{j=2,3} \frac{3}{16\pi}\frac{M_1}{M_j}\frac{Im[(\lambda\lambda^\dagger)_{1j}^2}{|\lambda\lambda^\dagger|_{11}} \tag{6.20}$$

If heavy neutrinos are quasi-degenerate (QD) for $\Delta M_{12}^2 = \Gamma_2^2$ and $M_3 >> M_{1,2}$ then [12],

$$\epsilon_1 = \frac{3}{4\pi}\frac{Im[(\lambda\lambda^\dagger)_{12}^2}{|\lambda\lambda^\dagger|_{11}}(\ln 2 - 1), \tag{6.21}$$

where it is easy to obtain a large ϵ_1. At last, to find η, the efficiency factor, one needs to solve for the Boltzmann equation, this time with new relevant Feymann processes (Figure 6.1) in contrast to the Type I Seesaw (Figure 4.1). Since the heavy

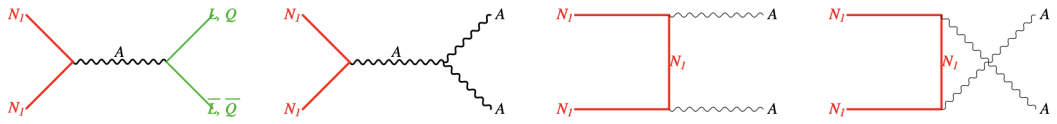

Figure 6.1: Additional Feynman diagrams must be added to the Boltzmann equation [12].

leptons have gauge interactions, they can easily achieve thermal equilibrium with other SM particles. Then Y_N^{eq} is explicitly found by counting relativistic particle content in the model. Overall, in the Type III model [12],

$$\frac{n_B}{n_\gamma} = -0.029\epsilon_1\eta. \tag{6.22}$$

These heavy leptons quickly decouple with others at a lower temperature and decay out of thermal equilibrium. Thus, one can have a large efficiency factor η compared to a type I seesaw (heavy neutrinos are "sterile").

Chapter 7

Testing Leptogenesis & the Seesaw Mechanism

As seen, the three (Type I, II and III) seesaw mechanisms explicitly explain the smallness of the neutrino masses and the BAU through Leptogenesis. Here, we will focus on the most widely studied seesaw mechanism, the low-scale Type I seesaw mechanism. Furthermore, the implications of the Type II and Type III seesaw mechanisms in experiments will be examined.

7.1 Testing the Type I Seesaw (The Low Scale Seesaw)

The crucial characteristic of the Type I seesaw [14] mechanism is the inclusion of RH neutrino fields, which are added as $SU(2)_L$ singlets to the SM without affecting the general properties. The minimal setup in which Leptogenesis is successful is a Type I Seesaw extension with 2 RH neutrinos and correspondingly two heavy Majorana neutrinos N_j with definite masses $M_j > 0$ for $j = 1, 2$. In classical thermal leptogenesis with the Majorana neutrinos having a hierarchical mass spectrum, BAU due to the out-of-equilibrium decays of N_j (L, C and CP violating decays) occurs at scales around but a few orders of magnitude less than the scale of unification for the EW and strong interactions in GUT [14]. The scale of leptogenesis, as shown previously, is determined by the magnitude of the heavy Majorana masses. At present, high-scale leptogenesis experiments have many complications. However, the low-scale Type I seesaw can lead to the possibility that heavy Maj-neutrinos can have masses less than TeV scales, which shows the possibility of testing in colliders or low-energy experiments.

In resonant leptogenesis [45], BAU is produced solely by CP violating N_j and Higgs decays mediated by the neutrino Yukawa couplings with the heavy Majorana neutrino with $M_j < (\ll)1$ TeV. For simplicity, in the case of 2 RH neutrinos, the resonant regime occurs when 2 heavy Majorana neutrinos are a quasi-degenerate pair such that $M_2 - M_1 > 0$ and $M_2 \approx M_1$. Results in [46] show the possible N_1 and N_2 initial abundances at temperature $T_0 >> T_{sph}$, T_{sph} being sphaleron decoupling temperature (131.7 GeV^2). The authors demonstrated that in both cases, $N_{1,2}$ Thermal Initial Abundance (TIA) and $N_{1,2}$ Vanishing Initial Abundance (VIA), successful resonant leptogenesis is possible. The heavy Majorana neutrinos would take an accessible range $M_{1,2} \simeq 0.3 - 100$ GeV for VIA and $M_{1,2} \simeq 5.0 - 100$ GeV for TIA. Moreover, accessible for values of the charged and neutral current couplings (for the Heavy Majorana neutrinos) in the weak interaction Lagrangian, denoted $(RV)_{i\ell}, \ell = e, \mu, \tau$, $j = 1, 2$ [46], in the range $10^{-6} - 5 \times 10^{-5}$. In contrast, the BAU is generated through RH neutrino oscillations in the freeze-in leptogenesis mechanism [47]. Recently, the parameter space of the two scenarios was studied in a unified framework with 2 Majorana neutrinos [48].

This was extended in [49], where they studied a case of three quasi-degenerate heavy Majorana neutrinos $N_{1,2,3}$ with $M_{1,2,3} \simeq M$. The author's work spanned M between 50 MeV to 70 TeV, focusing on an NH or quasi-degenerate (QD) mass spectrum and considering vanishing and thermal initial conditions. They found that the range of the couplings for charged current (CC) and neutral current (NC) with $N_{1,2,3}$ is several orders larger than the two heavy Majorana neutrino case. For $N_{1,2,3}$ with masses sub-TeV scale and with a large range of couplings can be investigated in high precision experiments on charged lepton flavour violation (cLFV) searching for μ decays and μ to e conversion in nuclei [14].

In the three singlet RH neutrino setup (ν_{aR}) with a Type I seesaw mechanism leptogenesis model, the required lepton number charge L is not conserved by the Majorana mass and the Yukawa couplings involving Higgs doublets. Furthermore, the breaking of C and CP symmetries is also ensured.

If one starts in a diagonal mass basis of the ν_{aR} and the charged leptons $\ell^{\pm}$ ($\ell = e, \mu, \tau$), the neutrino Yukawa coupling and the seesaw Majorana mass terms are [46][48][49],

$$\mathcal{L}_{Y,M} = -(Y_{\ell i}\overline{\psi_{\ell L}} i\tau_2 \Phi^*(x) N_{iR}(x) + h.c.) - \frac{1}{2} M_i \overline{N_i}(x) N_i(x), \tag{7.1}$$

where $Y_{\ell i}$ is the Yukawa neutrino couplings (in chosen basis), $(\psi_{\ell L}(x))^T = (\nu_{\ell L}^T(x)\ \ell_L^T(x))$. $\nu_{\ell L}$ is the LH neutrino and ℓ_L is the LH charged lepton field.

Further, the Higgs field is Φ, and N_i is the heavy Majorana field. In this basis, the neutrino fields $\nu_{\ell L}^T(x)$ which contribute to the expressions for CC and NC in the weak interaction, are given by [14],

$$\nu_{\ell L} = \sum_i (1+\eta) U_{\ell i} \nu_{iL}(x) + \sum_j (RV)_{\ell j} N_{jL}(x), \tag{7.2}$$

where N_{jL} are the LH components of the field of the heavy neutrinos N_j, ν_{iL} are the LH components of the three light Majorana neutrinos v_i with mass m_i ($m_i \lesssim 0.5\,\text{eV} \ll M_j$). U is a three-by-three unitary matrix and $\eta = -(1/2)(RV)(RV)^\dagger$. The matrix R is determined by $R \cong M_D M_N^{-1}$, M_D and M_N are the seesaw Dirac and RH Majorana neutrino mass matrix ($M_D \ll M_N$). V is a unitary matrix diagonalising the Majorana mass matrix of heavy RH neutrino M_N [14]. The matrix M_D (as shown in Chapter 4) is related to the Yukawa couplings Y by $M_D = (v/\sqrt{2})YV^T$. The Majorana mass matrix of the LH flavour neutrinos is given by

$$(m_v)_{\ell\ell'} \cong -[M_D M_N^{-1} (M_D)^T]_{\ell\ell'} = -\frac{v^2}{2} Y_{\ell j} M_j^{-1} Y_{j\ell'}^T = (U \tilde{m_v} U^T)_{\ell\ell'}. \tag{7.3}$$

where $\tilde{m_v}$ is a diagonal mass matrix for the light neutrinos. In this case, the PMNS matrix takes the form [14],

$$U_{PMNS} = (1+\eta)U, \tag{7.4}$$

where the matrix η describes the deviations from unitarity of the U_{PMNS}. The elements of η are constrained by EW data and data on flavour observables [50] [51]. Given the upper bounds on the elements of η are strong, $U_{PMNS} \approx U$. Here use the PMNS matrix with two Majorana phases, α_{21} and α_{31} [52],

$$\begin{pmatrix} c_{12}c_{13} & s_{12}c_{13} & s_{13}e^{-i\delta} \\ -s_{12}c_{23} - c_{12}s_{13}s_{23}e^{i\delta} & c_{12}c_{23} - s_{12}s_{13}s_{23}e^{i\delta} & s_{23}c_{13} \\ s_{12}s_{23} - c_{12}s_{13}c_{23}e^{i\delta} & -c_{12}s_{23} - s_{12}s_{13}c_{23}e^{i\delta} & c_{23}c_{13} \end{pmatrix} \begin{pmatrix} 1 & 0 & 0 \\ 0 & e^{\frac{i\alpha_{21}}{2}} & 0 \\ 0 & 0 & e^{\frac{i\alpha_{31}}{2}} \end{pmatrix}. \tag{7.5}$$

α_{21} and α_{31} cannot be constrained by neutrino oscillation experiments (treated as free parameters).

The quantities $(RV)_{\ell j}$ in equation 7.2 describe the strength of the CC and NC interactions with N_j to the $W^\pm$ bosons and the charged lepton ℓ and the Z boson

with the LH neutrino $\nu_{\ell L}$. Here, the weak Lagrangian is [14],

$$\mathcal{L}^{N}_{CC} = -\frac{g}{2\sqrt{2}}\overline{\ell}\gamma_{\alpha}(RV)_{\ell j}(1-\gamma_{5})N_{j}W^{\alpha} + h.c \tag{7.6}$$

$$\mathcal{L}^{N}_{NC} = -\frac{g}{4c_{w}}\overline{\nu_{\ell L}}\gamma_{\alpha}(RV)_{\ell j}(1-\gamma_{5})N_{j}Z^{\alpha} + h.c, \tag{7.7}$$

where $c_w = cos\theta_w$ and θ_w is the weak mixing angle. The magnitude of the coupling in the leptogenesis parameter range is crucial for low-scale leptogenesis testing. As shown in Chapter 4 in the CIP, the Yukawa coupling is described as [14],

$$Y = i\frac{\sqrt{2}}{v}U\sqrt{\tilde{m_{v}}}O^{T}\sqrt{\tilde{M}}, \tag{7.8}$$

where O is a complex orthogonal matrix, $O^{T}O = OO^{T} = I$, and $\tilde{M}$ is the diagonal mass matrix for the heavy Majorana neutrinos. The parameterization of O is given by $\theta_j = \omega_j + i\xi_j$ with $j = 1, 2, 3$ and ω_j, $\xi_j \in R$ for any j [46][48]. Thus,

$$O = \begin{pmatrix} c_2c_3 & c_2s_3 & s_2 \\ -s_1s_2c_3 - c_1s_3 & -s_1s_2s_3 + c_1c_3 & s_1c_2 \\ -c_1s_2c_3 + s_1s_3 & -c_1s_2s_3 - s_1c_3 & c_1c_2 \end{pmatrix}, \tag{7.9}$$

where $s_j = \sin\theta_j$ and $c_j = \cos\theta_j$. An alternative parametrization is [49],

$$O = (O_v R_C O_N)^{T}, \tag{7.10}$$

where $O_v = O_v^{12}O_v^{23}$ and $O_N = O_N^{23}O_N^{13}$ represent products of real rotations in the 1-2 and 1-3 planes, respectively. $R_C = R_C^{12}$ outlines a rotation by a complex angle in the 1-2 plane. The parametrization used provides convenience in the 3 RH Majorana case as it also involves a complex angle θ_C (in R_C). The authors worked in the extended range of the Majorana phases to account for both cases of $det(O) = \pm 1$ [14].

The results in [49] in the three RH neutrino cases with QD Majorana neutrinos with $M_{1,2,3} < 70$ TeV show that one can have Leptogenesis for either NH or QD light neutrino masses for M in the range 1.7 GeV - 70 TeV (TIA) and 50 MeV - 70 TeV (VIA). The Majorana neutrino couplings $\sum_{\ell j}|(RV)_{\ell j}|^2$ vary widely, with values that can be observed in low-energy experiments. e.g. for $m_1 = 0$ at NH, $M = 100$ GeV (70 TeV) then [49] shows $\max(\sum_{\ell j}|(RV)_{\ell j}|^2) \simeq 0.1(10^{-5})$. As shown in the equations, $\sum_{\ell j}|(RV)_{\ell j}|^2$ has a strong dependence on θ_C, mild dependence on CIP real angles and weak dependence on the Dirac and Majorana phases.

The CC and NC couplings in equation 7.6 and 7.7 provoke cLFV process in $\mu^{\pm} \to e^{\pm} + \gamma$, $\mu^{\pm} \to e^{\pm} + e^{+} + e^{-}$ and $\mu - e$ conversion in nuclei [16]. The branching ratios depend on the quantity $\sum_{i=1,2,3} |(RV)^{*}_{\mu i}(RV)_{ei}|^2$ and for $|M_i - M_j| \ll M_k, i \neq j = 1,2,3, k = 1,2,3$ on $M_{1,2,3} \simeq M$ of $N_{1,2,3}$ heavy Majorana neutrinos. The expressions for $BR(\mu^{\pm} \to e^{\pm} + \gamma)$, $BR(\mu^{\pm} \to e^{\pm} + e^{+} + e^{-})$ and $CR(\mu^{A}_{Z}X \to e^{A}_{Z}X)$ are the following [14] (3 QD Model):

$$BR(\mu \to e\gamma) = \frac{\Gamma(\mu \to e\gamma)}{\Gamma((\mu \to e + \nu_{\mu} + \overline{\nu_{e}})} = \frac{3\alpha_{EM}}{32\pi}|T|^2, \tag{7.11}$$

, where α_{em} is the fine structure constant and

$$T \cong [G(X) - G(0)] \sum_{i=1,2,3} (RV)^{*}_{\mu i}(RV)_{ei}. \tag{7.12}$$

$G(X)$ is a loop integration function and $X = (M/M_W)^2$ (Asummed $M_{1,2,3} \cong M$). The function $G(X)$ is monotonic and takes values in the range $[4/3, 10/3]$ with $G(X) \cong 10/3 - X$ for $X \ll 1$ (G(X) function found in [16]). Then [16] for (2RHN Model for simplicity),

$$\begin{aligned} CR(\mu^{A}_{Z}X \to e^{A}_{Z}X) &= \frac{\Gamma(\mu^{A}_{Z}X \to e^{A}_{Z}X)}{\Gamma_{capt}} \\ &= \frac{\alpha^{5}_{em}}{2\pi^4 \sin^4\theta_w}\frac{Z^{4}_{eff}}{Z}|F(-m^{2}_{\mu})|\frac{G^{2}_{F}m^{5}_{\mu}}{\Gamma_{capt}}|(RV)^{*}_{\mu 1}(RV)_{e1}||C_{\mu e}|^2. \end{aligned} \tag{7.13}$$

where Z is the proton number of the nucleus X, $\sin^2\theta_W = 0.23$, $F(-m^{2}_{\mu})$ is the nuclear form factor at momentum transfer squared of the muon mass, Z_{eff} is the effective atomic charge and Γ_{capt} is the experimentally known muon (total) capture rate. Further, $C_{\mu e}$ is the loop integral factor that shows the contributions from γ-penguin, Z-penguin and box-type diagrams. Finally for $\mu^{\pm} \to eee$ [16] (2RHN Model for simplicity),

$$BR(\mu \to 3e) = \frac{\alpha^{2}_{EM}}{16\pi^2 \sin^4\theta_W}|(RV)^{*}_{\mu 1}(RV)_{e1}||C_{\mu 3e}(x)|^2, \tag{7.14}$$

where $|C_{\mu 3e}(x)|^2$ decay factor is defined in reference [16]. Even though the rates of the cLFV τ decays are also proportional to the couplings, the sensitivity of experiments on $\tau^{\pm}$ decays are less stringent [14]. The $C_{\mu e}$ loop integral values, the $C_{\mu 3e}$ decay factor, and the Z proton number. From nuclear factor, $F(-m^{2}_{\mu})$, effective atomic charge and total capture rate can be found in reference [16].

Table 7.1: Current experimental constraints for μ processes

Parameter	Senisitivty	Reference
$BR(\mu^{\pm} \to e^{\pm} + \gamma)$	$< 4.2 \times 10^{-13}$	MEG [53]
$BR(\mu^{\pm} \to e^{\pm} + e^{+} + e^{-})$	$< 1.0 \times 10^{-12}$	SINDRUM I [54]
$CR(\mu^{A}_{Z} Ti \to e^{A}_{Z} Ti)$	$< 4.3 \times 10^{-12}$	SINDRUM II [55]
$CR(\mu^{A}_{Z} Au \to e^{A}_{Z} Au)$	$< 7.0 \times 10^{-13}$	SINDRUM II [56]

It has been shown that $\mu^{\pm} \to e^{\pm}+\gamma$, $\mu^{\pm} \to e^{\pm}+e^{+}+e^{-}$ and $\mu-e$ conversion in nuclei branching fractions are proportional to the couplings in Type I Seesaw Models, for the full derivations refer to [57] [16] [58]. The most stringent experimental limits on $\mu \to e\gamma$, $\mu \to eee$ and $\mu - e$ conversion in nuclei have been reported by MEG, SINDRUM and SINDRUM II collaborations as shown in Table 7.1

The MEG II (developing of MEG) aims to reach a sensitivity of $BR(\mu^{\pm} \to e^{\pm}+\gamma) \simeq 6.0 \times 10^{-14}$ [59]. Further, the Phase I (Phase II) of the Mu3e Project [60] plans to reach a sensitivity of $BR(\mu^{\pm} \to e^{\pm} + e^{+} + e^{-}) \sim 10^{-15}(10^{-16})$. Finally, the Mu2e [61] and COMET [62] collaboration studying $\mu - e$ conversion in aluminium aim to reach $CR(\mu^{A}_{Z} Al \to e^{A}_{Z} Al) \sim 6.0 \times 10^{-17}$ and the experiment PRISM/PRIME [63] aims to reach a sensitivity of $CR(\mu^{A}_{Z} Ti \to e^{A}_{Z} Ti) \sim 10^{-18}$.

For the $BR(\mu^{\pm} \to e^{\pm} + \gamma)$ at $M = M_W$ ($M = 1000$ GeV), one finds $G(X) - G(0) = -0.5(\simeq -1.9)$ [14] hence using equation 7.11 and 7.12 the MEG II will reach $\sum_{i=1,2,3} |(RV)^{*}_{\mu i}(RV)_{ei}| \gtrsim 3.3 \times 10^{-5}$ (8.9×10^{-6}) [14]. This value is 1 to 3 orders of magnitude smaller than $\max(\sum_{i=1,2,3} |(RV)^{*}_{\mu i}(RV)_{ei}|)$ at $M = M_W$ ($M = 1000$ GeV) for which for both TIA and VIA three QD Majorana low scale leptogenesis is possible.

For the $BR(\mu^{\pm} \to e^{\pm} + e^{+} + e^{-})$ at Mu3e experiment which is planning to reach $BR(\mu^{\pm} \to e^{\pm} + e^{+} + e^{-})$ around 10^{-15} (10^{16}) [60]. Thus smaller value of $\sum_{i=1,2,3} |(RV)^{*}_{\mu i}(RV)_{ei}|$ can be tested [14].

For the $CR(\mu^{A}_{Z} X \to e^{A}_{Z} X)$ at Mu2e, COMET and PRISM/PRIME, Mu2e [61] and COMET [62] are trying to reach a sensitivity of Aluminium, $CR(\mu^{27}_{13} Al \to e^{27}_{13} Al)$ around 6×10^{-17}. Which can be used to achieve smaller values of $\sum_{i=1,2,3} |(RV)^{*}_{\mu i}(RV)_{ei}|$. In the PRISM/PRIME experiment aiming at 10^{-18} [63] for the $\mu - e$ conversion rate in Titanium, one can achieve values of $\sum_{i=1,2,3} |(RV)^{*}_{\mu i}(RV)_{ei}|$ as small as 10^{-7} at $M \sim 100$ GeV [14].

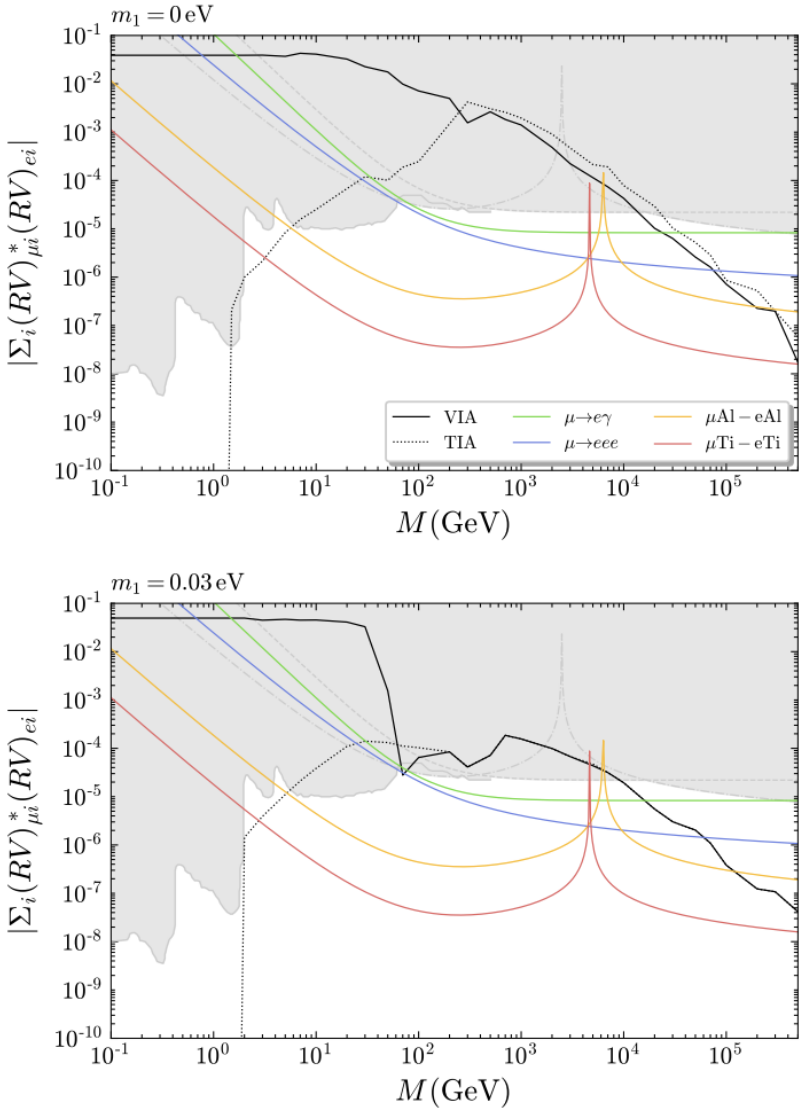

Figure 7.1: The region of successful Leptogenesis in the $\sum_{i=1,2,3} |(RV)^*_{\mu i}(RV)_{ei}| - M$ in case of a NH with $m_1 = 0$ is the top graph, and for Normal ordering (NO) with $m_1 = 0.03$ eV is the graph at the bottom. The solid and dotted black curves are the constraints (in VIA and TIA, respectively) for successful Leptogenesis. The grey region that extends to $M \sim 500$ GeV is excluded by low energy experiments [64]. The dashed contour is excluded by the upper limit of $BR(\mu \to e\gamma) < 4.2 \times 10^{-13}$ and the dot-dashed contour is excluded by $CR(\mu^{27}_{13}Au \to e^{27}_{13}Au) < 7 \times 10^{-13}$. The green, blue, yellow, and red lines belong to the sensitivity of upcoming $\mu^{\pm} \to e^{\pm} + \gamma$, $\mu^{\pm} \to e^{\pm} + e^{+} + e^{-}$ and $\mu - e$ conversion in nuclei experiments (Al and Ti) [14].

The authors [14] obtained a viable leptogenesis range in terms of cLFV observables by solving the density matrix equations and scanning the parameter space for the largest allowed values of $\sum_{i=1,2,3} |(RV)^*_{\mu i}(RV)_{ei}|$. In Figure 7.1 the regions of viable low-scale leptogenesis are shown in the $\sum_{i=1,2,3} |(RV)^*_{\mu i}(RV)_{ei}| - M$ plane for values greater or equal to 10^{-11} for the couplings and M in $0.1 - 5 \times 10^5$ GeV in the TIA and VIA cases. Regions below the dotted and solid lines, respectively. (The mass spectrum for light neutrinos is assumed to be normal ordering).

The lightest neutrino mass is set to $m_1 = 0$ for the top graph and $m_1 = 0.03$ eV for the bottom graph. Current low-energy data exclude the subregion [64], and limitations on the branching fractions of $BR(\mu^\pm \to e^\pm + \gamma)$ and $CR(\mu^A_Z X \to e^A_Z X)$ are shown in grey. The yellow and red lines represent the sensitivity of the future $\mu^\pm \to e^\pm + \gamma$, $\mu^\pm \to e^\pm + e^+ + e^-$ and $\mu^A_Z X \to e^A_Z X$ (for Ti and Al) experiments.

The figures indicate that future μLFV experiments can directly test crucial regions of the leptogenesis parameter space. As shown, the future MEG II can test the region from $M \cong 90$ GeV to $M \cong 2 \times 10^4$ GeV, and the Mu3e can test $M \cong 60$ GeV to $M \cong 7 \times 10^4$ GeV in the VIA case (For the TIA case slightly larger values) [14]. They will test values down to $\sum_{i=1,2,3} |(RV)^*_{\mu i}(RV)_{ei}| \sim 8 \times 10^{-6}$ and $\sum_{i=1,2,3} |(RV)^*_{\mu i}(RV)_{ei}| \sim 1.5 \times 10^{-6}$, respectively.

In the VIA (TIA) case the upcoming experiments on $\mu - e$ conversion in Al from Mu2e and COMET will be able to test the region between $M \simeq (4(6) - 3 \times 10^5)$ GeV and values of up to $\sum_{i=1,2,3} |(RV)^*_{\mu i}(RV)_{ei}| \sim 2 \times 10^{-7}$ [14]. PRISM/PRIME will test a region between $M \simeq (2(3) - 5 \times 10^5)$ GeV and up to $\sum_{i=1,2,3} |(RV)^*_{\mu i}(RV)_{ei}| \sim 1.6 \times 10^{-8}$ [14].

If one finds a positive result in the μLFV experiments, it will support a low-scale leptogenesis scenario with three (RH) QD-heavy Majorana neutrinos. From the data of μ decays, one can compute M and $\sum_{i=1,2,3} |(RV)^*_{\mu i}(RV)_{ei}|$ [14]. This permits us to make specific calculations on the branching fractions of the other processes. Note that in the region of the parameter space successful leptogenesis, the heavy Majorana neutrinos can simultaneously have sizeable CC couplings to the electron and muon and to the e, μ, τ [14].

In summary, upcoming and future μLFV experiments on $\mu^\pm \to e^\pm + \gamma$, $\mu^\pm \to e^\pm + e^+ + e^-$ and $\mu - e$ conversion in nuclei in Ti and Al can probe directly regions of viable low-scale leptogenesis parameter space based on type I with 3 QD heavy Majorana neutrinos. Furthermore, experiments on $\tau \to eee(\mu\mu\mu)$ and $\tau \to e(\mu)\gamma$ can probe parts of the parameter space (i.e. BaBar [65], BELLE II [66]).

7.2 Sensitivities of the $BR(\mu \to e\gamma)$

Table 7.2: Constraints for $BR(\mu \to e\gamma)$

Parameter	Senisitivty	Reference
$BR(\mu^{\pm} \to e^{\pm} + \gamma)$	$< 4.9 \times 10^{-11}$	Crystal Box [67]
$BR(\mu^{\pm} \to e^{\pm} + \gamma)$	$< 1.2 \times 10^{-11}$	MEGA [68]
$BR(\mu^{\pm} \to e^{\pm} + \gamma)$	$< 4.3 \times 10^{-12}$	MEG [53]

In the light of the 3 QD Low Scale Seesaw, the Crystal Box experiment [67] was operational in Los Alamos, USA, during the 1980s. Running at 4×10^{12} μ/s of beam intensity, the experiment collected the statistics of 1.4×10^{12} muons (stopped on target). Using a Maximum likelihood technique in a parameter space with four discriminating variables, they achieved the first limit shown in Table 7.2. Using equation 7.11 and 7.12, (at $M = M_W$ ($M = 1000$ GeV), with $G(X) - G(0) = -0.5(\simeq -1.9)$) the Crystal Box would have reached a sensitivity of $\sum_{i=1,2,3} |(RV)^*_{\mu i}(RV)_{ei}| \gtrsim 9.5 \times 10^{-4}$ (2.5×10^{-4}) (Calculation done by Author of this Dissertation).

The MEGA experiment [68] was operational in Los Alamos, USA, for about 10 years, and it could exploit a much larger beam rate up to 4×10^7 μ/s. The experiment collected data for three years for a total of 8×10^6s of live time and 1.2×10^{14} muons stopped on target. They achieved the second limit shown in Table 7.2. Using equation 7.11 and 7.12, (at $M = M_W$ ($M = 1000$ GeV), with $G(X) - G(0) = -0.5(\simeq -1.9)$) the MEGA would have reached a sensitivity of $\sum_{i=1,2,3} |(RV)^*_{\mu i}(RV)_{ei}| \gtrsim 4.7 \times 10^{-4}$ (1.2×10^{-4}) (Calculation done by Author of this Dissertation).

Finally, the MEG [53] experiment gives the best constraint with an innovative liquid Xenon calorimeter. (With a better resolution and time than the MEGA photon conversion approach). The experiment run at PSI, 3×10^7 μ/s collecting up to 7.5×10^{14} muons stopped on target. They achieved the last limit shown in Table 7.2. Using equation 7.11 and 7.12, (at $M = M_W$ ($M = 1000$ GeV), with $G(X) - G(0) = -0.5(\simeq -1.9)$) the MEG would have reached a sensitivity of $\sum_{i=1,2,3} |(RV)^*_{\mu i}(RV)_{ei}| \gtrsim 2.8 \times 10^{-4}$ (7.4×10^{-5}) (Calculation done by Author of this Dissertation).

Compared to the new sensitivity MEG II [59] will reach $BR(\mu^{\pm} \to e^{\pm} + \gamma) \simeq 6.0 \times 10^{-14}$, the limit in the couplings is improved significantly.

7.3 Type I Seesaw Leptogenesis at High Energies

Leptogenesis in a Type I Seesaw mechanism can also be realized in a high-scale leptogenesis mechanism, e.g. the out-of-equilibrium decay of heavy RH neutrinos with CP-violating processes. However, the RH neutrino masses are typically beyond the reach of current and future colliders (Except for resonant leptogenesis) [69]. Thus, these scenarios are difficult to experiment on.

One can "falsify" high-scale leptogenesis models via LNV around the TeV scale to probe models at high scales [69]. i.e., the observation of a same-sing dilepton signature without missing energy at the LHC implies a strong washout that an asymmetry at a high scale would be directly washed out before the sphaleron process. For leptogenesis scenarios around the TeV scale, observation of such a signal would imply a lower limit on the CP asymmetry [69].

Neutrinoless double beta decay ($0\nu\beta\beta$) is an LNV observable; if a new physics mechanism of $0\nu\beta\beta$ is found other than light neutrino exchange, one can exclude high-scale leptogenesis unless the baryon asymmetry is protected via another mechanism. Thus, if $0\nu\beta\beta$ is found, investigation of the underlying mechanism is significant [69]. Observations in all flavour sectors or an additional measurement of LNV are needed to confirm washout in all flavour sectors. In the case of $0v\beta\beta$, no confirmation has been found since the controversial Heidelberg-Moscow [70] results. Since then, neither has NEMO-3 [71] or GERDA [72] found a signal.

Depending on the new UV physics hierarchy, collider probes or $0\nu\beta\beta$ can have a larger experimental reach [69]. In addition, $0\nu\beta\beta$ is limited to only the first generation of leptons. Collider search allows for signatures in the second and third generation of leptons. Observing LNV at current or future colliders or $0\nu\beta\beta$ decay experiments would imply that single-flavour high-scale leptogenesis is inadequate [69].

Overall, experimental searches of LNV signatures are crucial for realising high-scale leptogenesis, even though the physics is accessible implicitly. Thus, observing LNV at $0\nu\beta\beta$ decay experiments via a non-standard mechanism or at current and future colliders can tend towards low energy scale scenarios. .

7.4 Implications of the Type II Seesaw

An essential characteristic of the Type II Seesaw model [11] is the inclusion of a $SU(2)_L$ triplet scalar Δ with a hypercharge of 1 to the SM without affecting the SM's general properties. In Type II, Δ has a non-zero VEV and the lepton sector couples to the triplet Higgs. Thus, the mass of the neutrinos can form. In addition, the Type II model can provide a mechanism for Leptogenesis by playing the role of inflation, as shown in Chapter 5. The model allows the triplet Higgs mass parameter to be as light as the TeV scale, which can be tested in the LHC and new collider experiments [15].

The LHC has performed surveys for the doubly charged Higgs contained in the triplet Higgs and currently sets a limit of around a few 100 GeV, depending on its decay products [73]. Its decay is sensitive to the VEV value of the triple Higgs. But if the model generates the BAU, a VEV less than 1 keV is preferred to avoid the lepton number being washed out [15]. Thus, one can look for the triple Higgs decay in the leptonic channel.

In this extension [15] of the SM through the addition of Δ, after EWSB, beyond the SM Higgs, there are six additional scalars in the model, identified as $A^0, H^0, H^{\pm}, H^{\pm\pm}$. A^0 and H^0 are the extra CP odd/even neutral scalars and $H^{\pm}$ and $H^{\pm\pm}$ are the charged Higgs and doubly charged Higgs respectively. Through a Drell-Yan process, the charged Higgs and the doubly charged Higgs can be pair-produced. Thus, one can look for channels to test the triplet Higgs in colliders. Depending on the number of observed leptons, we have the four-lepton channel, the three-lepton channel and the two-lepton channel [15] (each one with a different sensitivity). Then, through a combination of the three channels, the final result is derived. The triplet Higgs is a triplet in the SM group. Therefore, the charged Higgs and the doubly-charged Higgs can be produced together (the production rate can be higher than $H^{\pm\pm}$ pair-production). $H^{\pm\pm}H^{\mp}$ will contribute to the search channels in the LHC if the charged Higgs decay emits a lepton and a neutrino. Further, in the $H^{\pm\pm}H^{\mp}$ pair production, since the charged Higgs decay emits a lepton and a neutrino, a large missing energy will be undetected. Hence, one can search the $H^{\pm\pm}H^{\mp}$ decay via the signal of 3 electrons plus the missing energy (May have good sensitivity).

As shown in Chapter 5, the model contains the SM Higgs Doublet H and the $SU(2)_L$ scalar triplet Δ, which both have nonvanishing VEVs, as in equation 5.1. An additional Yukawa interaction modifies the Lagrangian as in equation 5.2, and we have a new potential as given in equation 5.4. After EWSB one finds (as in

reference [15]): a doubly charged Higgs $H^{\pm\pm}(=\Delta^{\pm\pm})$, two scalars $H^{\pm}$ and $G^{\pm}$ (which are combinations of $\Delta^{\pm}$ and $h^{\pm}$), the CP even neutral states H^0, h^0, and the CP odd states A^0, G^0. Here, $G^{\pm}$ and G^0 are the Goldstone bosons that form the longitudinal DOF of the $W^{\pm}$ and Z bosons.

The mass squared of the doubly charged Higgs is given by [15]

$$m^2_{H^{\pm\pm}} = \frac{\sqrt{2}\mu v_H^2 - 2\lambda_3 v \Delta^3 - \lambda_4 v_H^2 v_\Delta}{2v_\Delta}. \tag{7.15}$$

The mass squared of the charged Higgs is [15],

$$m^2_{H^{\pm}} = \frac{2\sqrt{2}\mu^2 + 4\sqrt{2}\mu v_\Delta^2 - \lambda_4 v_\Delta v_H^2 - 2\lambda_4 v_\Delta^3}{4v_\Delta}. \tag{7.16}$$

For the CP odd/even scalars, the mass is [15],

$$m^2_{H^0} = \frac{1}{2}[A + C + \sqrt{(A-C)^2 + 4B^2}], \tag{7.17}$$

$$m^2_{h^0} = \frac{1}{2}[A + C - \sqrt{(A-C)^2 + 4B^2}], \tag{7.18}$$

$$m^2_{A^0} = \frac{\mu(v_H^2 + 4v_\Delta^2)}{\sqrt{2}v_\Delta}. \tag{7.19}$$

Through equations 7.17 to 7.19,

$$A = \frac{\lambda}{2} v_H^2, \tag{7.20}$$

$$B = -\sqrt{2}\mu v_H + (\lambda_1 + \lambda_4) v_H v_\Delta, \tag{7.21}$$

$$C = \frac{\sqrt{2}\mu v_H^2 + 4(\lambda_1 + \lambda_4) v_\Delta^3}{2v_\Delta}. \tag{7.22}$$

In the limit $v_\Delta \ll v_H$, one finds the following relation [15],

$$m^2_{H^{\pm\pm}} - m^2_{H^{\pm}} \approx m^2_{H^{\pm}} - m^2_{H^0/A^0} \approx \frac{-\lambda_4 v_H^2}{4}. \tag{7.23}$$

Defining the mass-splitting parameter as $\Delta m = m_{H^{\pm\pm}} - m_{H^{\pm}}$ (mass difference of spectra in triplet Higgs sector). The decay behaviour of the triplet Higgs, for different parameter ranges [15], is $\Delta m < \mathcal{O}(10)$ GeV and $v_\Delta < 10^{-4}$ GeV, $H^{\pm\pm}/H^{\pm}$ decays into $\ell^{\pm\pm}/\ell^{\pm}\nu$. For $\Delta m < \mathcal{O}(10)$ GeV and $v_\Delta < 10^{-4}$ GeV, $H^{\pm\pm}/H^{\pm}$ decays into $W^{\pm\pm}/W^{\pm}Z$ or $W^{\pm}h^0$. If $\Delta m > \mathcal{O}(10)$, then one would find a cascade of decay channels. In the case of the Type II Seesaw Leptogenesis, for $\Delta m < \mathcal{O}(5)$ GeV and $v_\Delta < 10$ keV, the $H^{\pm\pm}/H^{\pm}$ would mainly decay into dileptons. Thus, one would

find a multi-lepton signature.

As shown in Chapter 5, the minimal Type-II Seesaw model through the AD mechanism can cause leptogenesis. The scalar field acquires a large VEV during the inflationary epoch in the AD mechanism. At the end of inflation, a lepton number asymmetry generated would be transferred to the baryon asymmetry.

Now consider the non-minimal couplings of Δ and H to gravity; the Lagrangian in the Jordan frame is equation 5.8 [11], where R is the Ricci scalar. The non-minimal couplings have the form of equation 5.9. Then, after a Weyl transformation, the Lagrangian is transferred into the Einstein frame (with an Einstien-Hilbert form the gravitational portion). Then the potential of the scalar, in Einstein frame, can be written as [15]

$$V_E(H,\Delta) = \frac{M_p^4}{(M_p^2 + 2F(H,\Delta))^2} V(H,\Delta), \tag{7.24}$$

which in the large field limit of h and Δ^0, one finds a flat direction. This flat direction is a Starobinsky-like inflation trajectory, and inflation is the mixing of h and Δ^0. As shown, Δ carries a lepton number of -2 and μ term-induced LNV (AD mechanism ingredients). Then, as shown in section 5.1, the AD mechanism generates a lepton number asymmetry, which is then transferred to baryon number forming BAU.

However, after reheating, LNV processes cannot be in thermal equilibrium since the generated lepton asymmetry would be washed out. Thus, one demands that $LL \longleftrightarrow HH$ and $HH \longleftrightarrow \Delta$ are not in thermal equilibrium [15],

$$\Gamma\big|_{T=m_\Delta} = n|\langle\sigma v\rangle \approx y^2\mu^2/m_\Delta < H\big|_{T=m_\Delta}, \tag{7.25}$$

$$\Gamma_{ID}(HH \longleftrightarrow \Delta)\big|_{T=m_\Delta} \simeq \frac{\mu^2}{32\pi m_\Delta} < H\big|_{T=m_\Delta}, \tag{7.26}$$

where

$$H\big|_{T=m_\Delta} = \sqrt{\frac{\pi^2 g_*}{90}}\frac{m_\Delta^2}{M_p}. \tag{7.27}$$

Using equations 7.27 and 7.26, to avoid washout one finds [15],

$$v_\Delta \lesssim 10^{-5}\ \text{GeV}\ (\frac{m_\Delta}{1\ \text{TeV}})^{-1/2}. \tag{7.28}$$

So for $m_\Delta \gtrsim 1$ TeV, one needs $v_\Delta \lesssim 10$ keV.

Through CC and NC Drell-Yan reactions, Δ Higgs can be created in the LHC [15],

$$q\overline{q} \xrightarrow{\gamma^*/Z^*} H^{\pm\pm}H^{\mp\mp}/H^{\pm}H^{\mp}/H^0A^0, \quad q\overline{q'} \xrightarrow{W^*} H^{\pm\pm}H^{\mp}/H^{\pm}H^0/H^{\pm}A^0. \tag{7.29}$$

The Feynmann diagrams for $H^{\pm\pm}H^{\mp\mp}$, $H^{\pm\pm}H^{\mp}$ are shown in Figure 7.2.

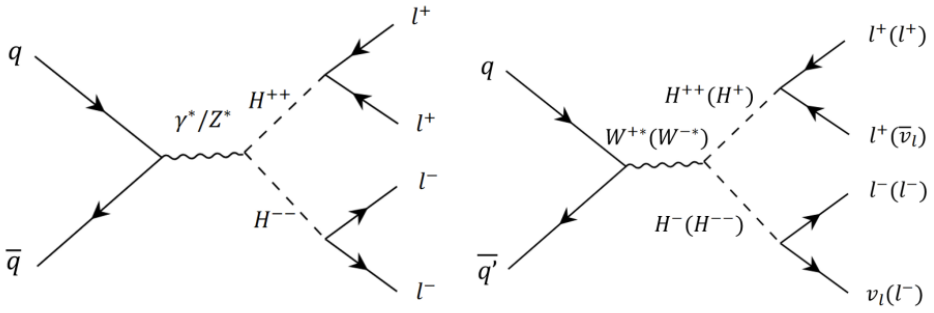

Figure 7.2: Feynman diagrams for $pp \to H^{\pm\pm}H^{\mp\mp}$ and $pp \to H^{\pm\pm}H^{\mp}$ [15]

Given the setup as in [15],

$$\begin{aligned} q(p_1) + \overline{q}(p_2) &\to H^{++}(k_1) + H^{--}(k_2), \\ q(p_1) + \overline{q'}(p_2) &\to H^{++}(k_1) + H^{-}(k_2), \end{aligned} \tag{7.30}$$

one finds the parton level cross-section to be [15],

$$\begin{aligned} \frac{d\sigma}{dy}(q\overline{q} \to H^{++}H^{--}) = \frac{3\pi\alpha^2\beta_1^3(1-y^2)}{N_c s}\Big(e_q^2 + \frac{s}{(s-M_Z)^2}\frac{\cos 2\theta_W}{\sin^2 2\theta_w} \\ \times\big[4e_q g_V^q(s-M_Z^2) + 4(g_V^{q2}+g_A^{q2})s\frac{\cos 2\theta_W}{\sin^2 2\theta_w}\big]\Big), \end{aligned} \tag{7.31}$$

$$\frac{d\sigma}{dy}(q\overline{q'} \to H^{++}H^{-}) = \frac{\pi\alpha^2\beta_2^3(1-y^2)}{16N_c\sin^4\theta_W}\frac{s}{(s-M_W^2)^2}. \tag{7.32}$$

Here $y = p_1 \cdot k_1$, s is the partonic centre of mass energy, and α is the QED coupling at scale $\sqrt{2}$, e_q is the electric charge of quark q. Further [15],

$$\beta_1 = \sqrt{1 - 4m_{H^{\pm\pm}}^2/s}, \tag{7.33}$$

$$\beta_2 = \sqrt{(1-(m_{H^{\pm}}+m_{H^{\pm\pm}})^2/s)(1-(m_{H^{\pm}}-m_{H^{\pm\pm}})^2/s)}. \tag{7.34}$$

In Figure 7.3 we show the cross-sections of both $H^{\pm\pm}H^{\mp\mp}$, $H^{\pm}H^{\mp}$ and $H^{\pm\pm}H^{\mp}$ from the collision of 2 protons against the mass of $H^{\pm\pm}$. Here, the authors [15] used a K-factor of 1.25 [74] and assumed that both $H^{\pm\pm}$ and $H^{\pm}$ carry the same mass parameter. As shown in the figure, $H^{\pm\pm}H^{\mp\mp}$ has a significant cross-section

and a distinct signature, i.e. the same lepton final state. However, $H^{\pm\pm}H^{\mp}$ has a greater cross-section than $H^{\pm\pm}H^{\mp\mp}$. Therefore, it can grant us a better channel for the Δ search.

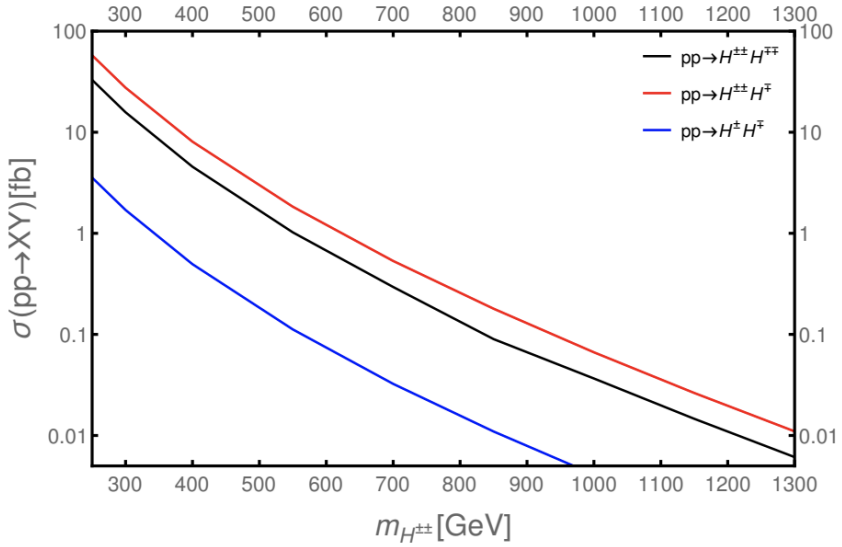

Figure 7.3: Pair production cross-section of the triplet scalars in a collider with $\sqrt{s} = 13$ TeV and $\Delta m = 0$ [15]

The authors in reference [15] considered the case where $\Delta m < \mathcal{O}(1)$ GeV and $v_\Delta < 10^{-6}$ GeV. Therefore, $H^{\pm\pm}$ and singly-charged scalars generally decay into leptonic final states. The branching ratios are [15],

$$BR(H^{\pm\pm} \to \ell_i^\pm \ell_j^\pm) = \frac{2}{1+\delta_{ij}} \frac{|y^v_{ij}|^2}{\sum_{mn} |y^v_{mn}|^2}, \tag{7.35}$$

$$BR(H^{\pm} \to \ell_i^\pm \nu_j) = \frac{|y_{ij}|^2}{\sum_{mn} |y_{mn}|^2}, \tag{7.36}$$

where y^v and y are defined as,

$$y^v = \frac{1}{\sqrt{2} v_\Delta} U diag(m_1, m_2, m_3) U^T, \tag{7.37}$$

$$y = \frac{\cos\beta}{v_\Delta} diag(m_1, m_2, m_3) U^T. \tag{7.38}$$

Here, U is the lepton mixing matrix measured in neutrino oscillations. Additionally, the leptonic BR depends on the mass hierarchy of the neutrinos. As shown in [75] [15],

$$\begin{aligned} NH: &\ \ BR(H^{++} \to \mu\mu), BR(H^{++} \to \tau\tau) \gg BR(H^{++} \to ee), \\ IH: &\ \ BR(H^{++} \to ee) \gg BR(H^{++} \to \mu\mu), BR(H^{++} \to \tau\tau). \end{aligned} \tag{7.39}$$

The authors then assumed that $BR(H^{++} \rightarrow ee) = 100\%$ for their study on multi-electron searches in LHC.

The ATLAS collaboration has experimented on multi-lepton final state searches at an integrated luminosity of $36.1 fb^{-1}$ of proton-proton collisions at the centre of mass energy of 13 TeV [76]. The author's [15] analysis focuses on the $H^{\pm\pm} \rightarrow e^{\pm}e^{\pm}$, $H^{\pm\pm} \rightarrow e^{\pm}\mu^{\pm}$, and $H^{\pm\pm} \rightarrow \mu^{\pm}\mu^{\pm}$ with a branching ratio around 100%. The events are classified into three different regions, and their chosen selection criteria are shown in Table 7.3.

Table 7.3: Selection Criteria [15]

Parameter	Two electrons	Three electrons	Four electrons
b-jet veto	YES	YES	YES
Z veto	NO	YES	YES
$P_T(e^{\pm}e^{\pm}) > 100$ GeV	YES	YES	NO
$\sum \lvert P_T(e)\rvert > 300$ GeV	YES	YES	NO
$\Delta R(e^{\pm}, e^{\pm}) < 3.5$ GeV	YES	YES	NO
$\Delta M/\overline{M}$	NO	NO	YES

Here P_T is transverse momentum, and ΔR separates the pair of particles. The final state that included two and three electrons is also considered due to the missing leptons in the detector. The authors [15] simulated the experimental process by adding the contribution of $H^{\pm\pm}H^{\mp}$ to the signal event ($H^{\pm\pm}H^{\mp}$ contributes to two and three electrons electron signal).

One requires at least a pair of same charge electrons for the two-electron and three-electron signal regions. The separation of the same-charge electrons must be ΔR less than 3.5, and the sum of P_T must be more than 300 GeV [15]. Further, the vector sum of P_T was selected greater than 100 GeV. The selection needed for the $e^{\pm}$ was $|\eta| < 2.47$ and $P_T > 30$ GeV. To reduce the Z production background, in the 3-electron and 4-electron signals, events were rejected if any opposite-charge electron (same flavour) pair was within 10 GeV of the Z boson. The 4-electron signal requires the two electron pairs to have the same charge and net charge of 0. Finally, $\Delta M/\overline{M}$ criteria are applied to exclude background from incompatible invariant masses of same-charge pairs, where $\Delta M = |m^{++} - m^{--}|$ and $\overline{M} = (m^{++} + m^{--})/2$ [15]. In ATLAS, one finds a different $\overline{M}$ for a ΔM value. In the 4-electron channel, the authors chose $\Delta M/\overline{M} < 0.1$. In the 2-electron, 3-electron and 4-electron channels, the invariant mass of the same-charge pairs must be greater than 200 GeV [15]. Additionally, events with b-tagged jets were vetoed to reduce background events from top-quark decays.

The authors [15] used a signal cut efficiency and CLs method [77] to validate the simulation and obtain a confidence level for the cross-section. The result of the full simulation is shown in Figure 7.4, where one can find the limit of ATLAS in the dotted black line (close to the one derived in the simulation).

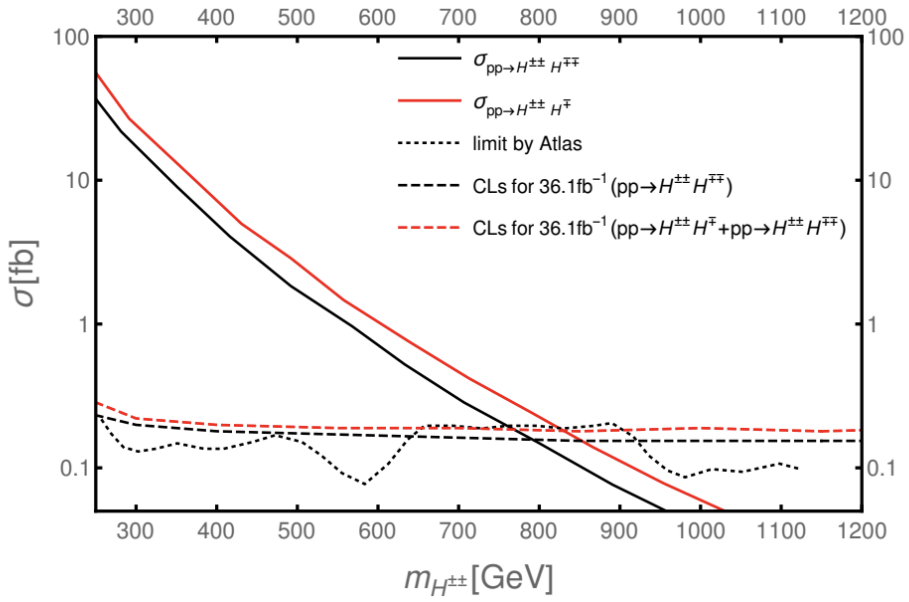

Figure 7.4: The limits for the branching ratios are (ee) 100%, ($e\mu$) 0%, ($\mu\mu$) 0%. The black and red solid lines show the cross-section of $pp \to H^{\pm\pm}H^{\mp\mp}$ and $pp \to H^{\pm\pm}H^{\mp}$, respectively [15]. The black dashed line is the 95% confidence level (Comparable to the limit by ATLAS [76], the black dotted line.) Combining both processes, one finds the red dashed line is the 95% confidence level.

Since $pp \to H^{\pm\pm}H^{\mp}$ contributes to the 2-electron and 3-electron signal, one expected the real limit to be stronger. Hence, the authors [15] simulated the process $pp \to H^{\pm\pm}H^{\mp} \to \ell^{\pm}\ell^{\pm}\ell^{\mp}\nu$ to compute signal efficiency. First, denoting the cross-section of $pp \to H^{\pm\pm}H^{\mp\mp}$ as σ_1 and its cut efficiency as ϵ_1 and denoting the cross-section of $pp \to H^{\pm\pm}H^{\mp}$ as σ_2 and its cut efficiency as ϵ_2. Then, the total signal is [15] ($\mathcal{L}$ here is luminosity, and they set a limit on total signal events)

$$n = \mathcal{L}\sigma_1\epsilon_1 + \mathcal{L}\sigma_2\epsilon_2. \tag{7.40}$$

The authors [15] then calculated an effective cut efficiency of

$$\epsilon_{2eff} = \epsilon_2 + \sigma_1/\sigma_2\epsilon_1 \tag{7.41}$$

for $pp \to H^{\pm\pm}H^{\mp}$ process. Thus, one can place a limit on the cross-section of $pp \to H^{\pm\pm}H^{\mp}$. The combined limit is roughly 100 GeV, greater than without it.

The $pp \to H^{\pm\pm}H^{\mp}$ has a greater cross-section, and missing energy is also embedded in the final states. Examining $3e + E_T^{miss}$, the relevant background for this signal is produced from diboson (ZZ, ZW, WW), $t\bar{t}$, $tt\overline{W}$, $tt\overline{Z}$, $tt\overline{h}$, triboson and Drell-Yan processes [15]. The other backgrounds are dominated by the background generated by the diboson (the only process considered in the simulation). The leading order cross-section for the diboson process [78] and the K-factor at a centre-of-mass energy of 13 TeV are shown in Table 7.3.

Table 7.4: Diboson Process and K-Factor [78]

Parameter	ZZ	W^+Z	W^-Z	WW
σ[pb]	9.89	15.51	9.53	67.74
K-factor	1.62	1.84	1.91	1.66

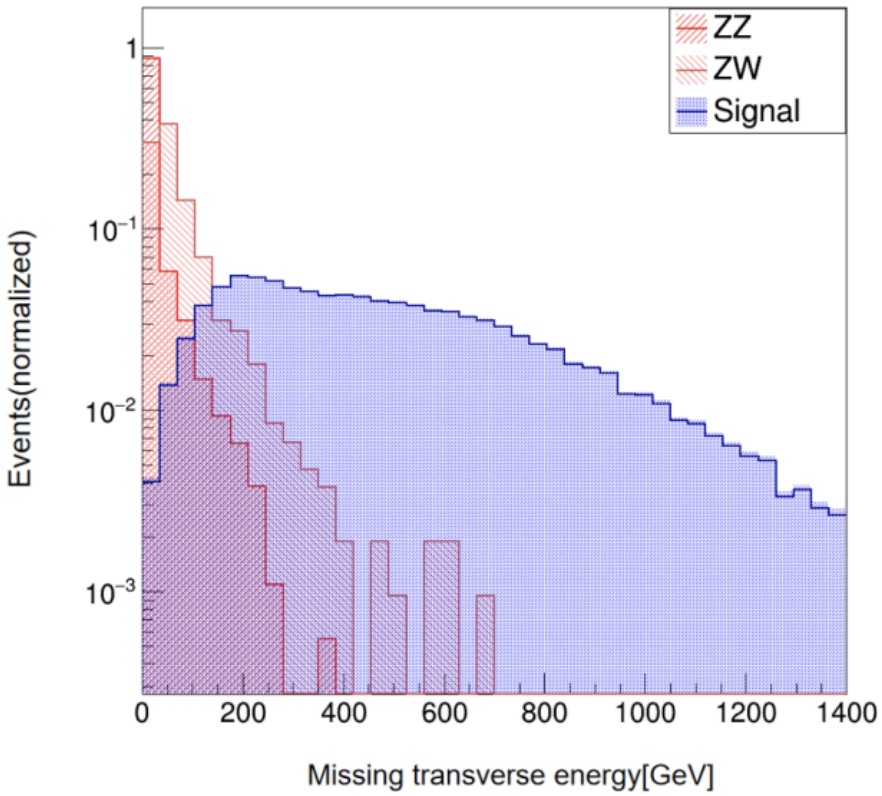

Figure 7.5: The missing transverse energy distribution of the process, $pp \to H^{\pm\pm}H^{\mp} \to \ell^{\pm}\ell^{\pm}\ell^{\mp}\nu$ with a Branching ratio for (ee) 100% overlapped by the diboson background (including pre-selection) [15]. The mass of the doubly charged Higgs and the singly charged Higgs is assumed to be around 1 TeV.

To ensure that the simulation is credible and check for a charge misidentification in the electron channel, the same charge region is considered (only b-jet veto). For $pp \to H^{\pm\pm}H^{\mp} \to \ell^{\pm}\ell^{\pm}\ell^{\mp}\nu$, a significant missing transverse energy will appear in

the final state due to the neutrino. A simulation of the missing energy distribution of the diboson process and $pp \to H^{\pm\pm}H^{\mp} \to \ell^{\pm}\ell^{\pm}\ell^{\mp}\nu$ is shown in Figure 7.5 [15]. As shown in Figure 7.5, a missing energy cut, roughly a few 100 GeV, would remove the background.

Due to the clear distinction of the missing energy distribution among the signal and diboson, the author [15] added a missing energy cut $E_T^{miss} > 300$ GeV. The total cut at a luminosity of $3000 fb^{-1}$ at 13 TeV is shown in [15]. Through the cut, only 10 percent of the diboson background remains. Using $S/\sqrt{B}$ (expected discovery significance), one finds Figure 7.6 at $3000 fb^{-1}$ at 13 TeV.

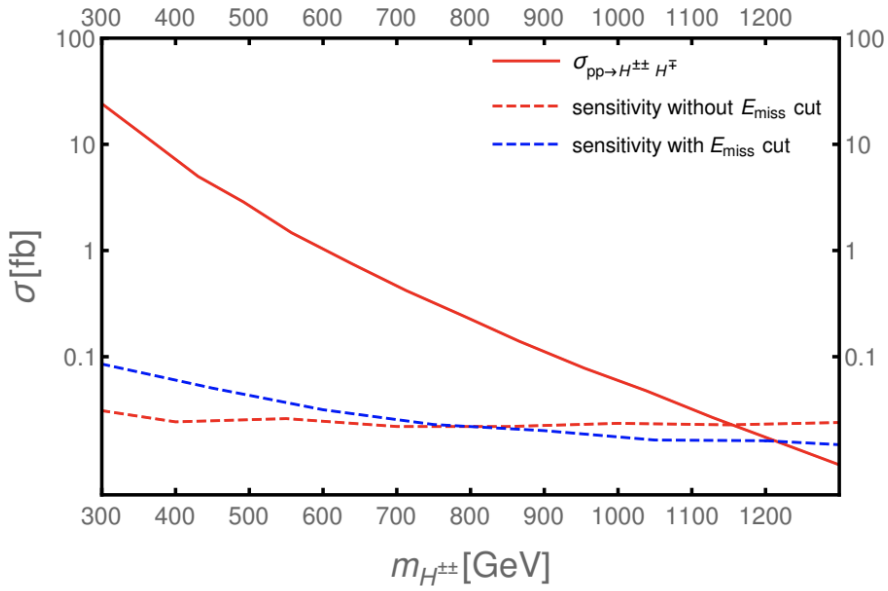

Figure 7.6: Future searches sensitivity at $3000 fb^{-1}$ [15]

One finds that for the triplet Higgs mass less than 1.2 TeV, the LHC for a high luminosity can reach a 2σ on the measurement. The graph also shows a comparison without the missing energy cut. The multi-electron channel provides better sensitivity when the triplet mass is below 800 GeV. But for greater than 800 GeV, the $3e + E_T^{miss}$ can measure a larger triplet Higgs mass. When the mass of the triplet Higgs is low, E_T^{miss} could be lower, hurting the signal [15]. Larger missing energy can further suppress the background and improve sensitivity.

Overall, the author [15] found $pp \to H^{\pm\pm}H^{\mp}$ can improve the sensitivty of multi-electron channels searching for $H^{\pm\pm}H^{\mp\mp}$ pair production. Furthermore, they found that the $3e + E_T^{miss}$ channel can provide better sensitivity for $pp \to H^{\pm\pm}H^{\mp}$ than the multi-electron channel. The future LHC could reach a mass around 1.2 TeV at 2σ level and luminosity of $3000 fb^{-1}$ in the $3e + E_T^{miss}$ channel.

7.5 Testing of the Type II Seesaw in Muon decays

Given a Type II Seesaw Lagrangian with a triplet Higgs as in equation 6.2 [16],

$$\mathcal{L}^{II}_{Seesaw} = -M^2_\Delta Tr(\Delta^\dagger\Delta) - \big(h_{\ell\ell'}\overline{\psi^C_{\ell L}} i\tau_2\Delta\psi_{\ell' L} + \mu_\Delta H^T i\tau_2\Delta^\dagger H + h.c\big). \tag{7.42}$$

where $(\psi_{\ell L})^T = (\nu^T_{\ell L}\ \ell^T_L)$ and $\overline{(\psi^C_{\ell L})} = (-\nu^T_{\ell L}C^{-1}\ -\ell^T_L C^{-1})$ and H are the SM lepton and Higgs doublet, C is the charge conjugation matrix, and μ_Δ is a parameter that characterizes the soft explicit breaking of total lepton number conservation.

The light neutrino mass matrix m_v relates the flavour structure of the Yukawa matrix h and μ_Δ (generated when the neutral element of Δ has a VEV). Setting $\Delta^0 = v_\Delta$ and $H^T = (0, v)^T$ where $v \simeq 174$ GeV, then from equation 7.42 [16],

$$(m_v)_{\ell\ell'} \simeq 2h_{\ell\ell'}v_\Delta. \tag{7.43}$$

Then the Yukawa matrix $h_{\ell\ell'}$ is directly proportional to U_{PMNS} [16],

$$h_{\ell\ell'} = \frac{1}{2v_\Delta}(U^* diag(m_1, m_2, m_3)U^\dagger)_{\ell\ell'}. \tag{7.44}$$

The amplitudes of the $\mu^\pm \to e^\pm + \gamma$, $\mu^\pm \to e^\pm + e^+ + e^-$ and $\mu - e$ conversion in nuclei, LFV processes in the Type II model are proportional at LO to the product of two elements in the Yukawa matrix h [16]. Thus, this relation implies that the rate of the LFV process is near the current upper limits and within the sensitivity of future experiments (for $\Delta M = 100 - 1000$ GeV and a small Higgs triplet VEV v_Δ, roughly 1-100 eV) [16]. A rather small v_Δ value implies a small value of μ.

The corresponding effective low-energy LFV Lagrangian, which contributes to the $\mu - e$ transition process, is written in the form [16],

$$\begin{aligned}\mathcal{L}^{eff} =& -4\frac{eG_F}{\sqrt{2}}(m_\mu A_R\overline{e}\sigma^{\alpha\beta}P_R\mu F_{\beta\alpha} + h.c.) \\ &- \frac{e^2G_F}{\sqrt{2}}(A_L(-m^2_\mu)\overline{e}\gamma^\alpha P_L\mu\sum_{Q=u,d}\overline{q_Q}\overline{Q}\gamma_\alpha Q + h.c).\end{aligned} \tag{7.45}$$

Here, e is the proton charge, $q_u = 2/3$ is the up quark electric charge, and $q_d = -1/3$ is the electric down quark charge. The form factors $A_{R,L}$, $F_{\alpha\beta}$, P_R, P_L and $\sigma^{\alpha\beta}$, G_F are defined in reference [16]. The term with the form factor A_R generates the $\mu^\pm \to e^\pm + \gamma$ decay amplitude, analogous to the contribution of the one-loop diagrams with a virtual neutrino and Δ^+ and with a virtual lepton and Δ^{++}. The terms A_L and A_R generate the conversion amplitude of $\mu - e$.

For the $\mu^{\pm} \to e^{\pm} + \gamma$ decay the authors [16] found that it is given by,

$$BR(\mu^{\pm} \to e^{\pm} + \gamma) \simeq 384\pi^2(4\pi\alpha_{em})|A_R|^2 = \frac{\alpha_{em}}{192\pi}\frac{|(h^{\dagger}h)_{e\mu}|^2}{G_F^2}(\frac{1}{m^2_{\Delta^+}} + \frac{8}{m^2_{\Delta^{++}}})^2. \tag{7.46}$$

Then for $m_{\Delta^+} \simeq m_{\Delta^{++}} = M_{\Delta}$, for a upper limit of $BR(\mu^{\pm} \to e^{\pm} + \gamma) < 2.4 \times 10^{-12}$ by MEG [79], implies [16],

$$|(h^{\dagger}h)_{e\mu}| < 5.8 \times 10^{-6}(\frac{M_{\Delta}}{100GeV})^2. \tag{7.47}$$

Moreover, one can use equation 7.47 to obtain a lower bound in the VEV of Δ^0, v_{Δ} using the following equation [16],

$$|(h^{\dagger}h)_{e\mu}| = \frac{1}{4v_{\Delta}^2}|U_{e2}U^{\dagger}_{2\mu}\Delta m^2_{21} + U_{e3}U^{\dagger}_{3\mu}\Delta m^2_{31}|. \tag{7.48}$$

For the $\mu^{\pm} \to e^{\pm} + e^{+} + e^{-}$ decay, the amplitude is generated at the tree level by a diagram with the exchange of a virtual Δ^{++}. Then the branching ratio is found to be [16],

$$BR(\mu^{\pm} \to e^{\pm} + e^{+} + e^{-}) = \frac{1}{G_F^2}\frac{|(h^{\dagger})_{ee}(h_{\mu e})|^2}{m^4_{\Delta^{++}}} = \frac{1}{G_F^2 m^4_{\Delta^{++}}}\frac{|m^*_{ee}m_{\mu e}|^2}{16v^4_{\Delta}}. \tag{7.49}$$

From the present limit limit $BR(\mu^{\pm} \to e^{\pm} + e^{+} + e^{-}) \sim 10^{-12}$ [54], then [16]

$$|(h^{\dagger}h)_{e\mu}| < 1.2 \times 10^{-7}(\frac{m_{\Delta^{++}}}{100GeV})^2. \tag{7.50}$$

Finally, for $\mu - e$ conversion in nuclei, the conversion rate is parametrized by the effective field theory approach in [80]. Taking into account the type II lagrangian then [16],

$$CR(\mu N \to eN) \simeq (4\pi\alpha_{em})^2\frac{2G_F^2}{\Gamma_{capt}}|A_R\frac{D}{\sqrt{4\pi\alpha_e m}} + 2(q_u + q_d)A_L V^{(p)}|^2. \tag{7.51}$$

Here, V and D depict the muon and electron wavefunction overlap integrals, and they are related to vector and dipole type operations in the Lagrangian.

For a light nucleus, i.e. for $Z \lesssim 30$, one can find an approximation $D \simeq 8\sqrt{4\pi\alpha_{em}}V^p$, with V^p, the vector type overlap integral of the proton, given by [16],

$$V^p \simeq \frac{1}{4\pi}m_{\mu}^{5/2}\alpha_{em}^{3/2}Z^2_{eff}Z^{1/2}F(-m_{\mu}^2), \tag{7.52}$$

where $F(q^2)$ is the form factor of the nucleus and α_{em} is fine structure constant.

The values of the parameters $Dm_\mu^{-5/2}, V^{(p)}m^{-5/2}$ and Γ_{capt} are given in [16]. The conversion rate can be written as [16],

$$\begin{aligned} CR(\mu N \to eN) \simeq & \frac{\alpha_{em}^5}{36\pi^4}\frac{m_\mu^5}{\Gamma_{capt}} Z_{eff}^4 Z F^2(-m_\mu^2)|(h^\dagger h)_{e\mu}|\big[\frac{5}{24m_{\Delta^+}^2}+\frac{1}{m_{\Delta^{++}}^2}\big] \\ & + \frac{1}{m_{\Delta^{++}}^2}\sum_{\ell=e,\mu,\tau}|h_{e\ell}^\dagger f(r,s_\ell)h_{\ell\mu}|^2, \end{aligned} \tag{7.53}$$

Here, the loop function $f(r, s_\ell)$ is defined in reference [16]. Thus assuming that $m_{\Delta^+} \cong m_{\Delta^{++}} = M_\Delta$ then $CR(\mu N \to eN) \propto |C_{\mu e}^{(II)}|^2$. $C_{\mu e}^{(II)}$ is defined as [16],

$$C_{\mu e}^{(II)} = \frac{1}{4v_\Delta^2}\big[\frac{29}{24}(m^\dagger m)_{e\mu} + \sum_{\ell=e,\mu,\tau} m_{e\ell}^\dagger f(r,s_\ell)m_{\ell\mu}\big]. \tag{7.54}$$

The upper limit of $CR(\mu Ti \to eTi) < 4.3 \times 10^{-12}$ [55] leads to [16],

$$|C_{\mu e}^{(II)}| < 1.24 \times 10^{-4}(\frac{M_\Delta}{100GeV})^2. \tag{7.55}$$

Taking the limit $m_{\Delta^{++}} \gg m_{\Delta^+}$ with $m_{\Delta^+} = (100 - 1000)$ GeV, then $|C_{\mu e}^{(II)}| \propto |(h^\dagger h)_{e\mu}|$ (the dominant contribution is the exchange of the singly charged scalar). Then [16],

$$|(h^\dagger h)_{e\mu}| < 6 \times 10^{-4}(\frac{m_{\Delta^+}}{100GeV})^2, \tag{7.56}$$

It produces a weaker upper bound than the one given by $\mu^\pm \to e^\pm + \gamma$.

Chapter 8

Discussion

The Type I, II and III Seesaw mechanisms simultaneously explain the minuteness of the neutrino mass and the BAU through different Leptogenesis mechanisms. As they extend the SM through different particles, their testing varies widely, from searching a triplet Higgs to searching for heavy Majorana neutrinos. As shown, seesaw model extensions lead to observable effects in μ decays and can even be observed through their decay products in collider experiments.

8.1 Kinship of Seesaw Models

Chapter 4 shows that the SM is extended by adding heavy Majorana RH neutrinos in the Type I Seesaw [10]. Including Majorana mass terms and Higgs-RH neutrino Yukawa term leads to the manifestation of a mass matrix, which can then be further diagonalized to obtain the masses of the particles. If one is restricted to the seesaw limit, one finds an expression relating the light masses with the heavy masses where the Yukawa couplings and large RHN masses suppress the light neutrino mass. This is analogous to a Seesaw; the light masses decrease if the RHN masses increase. Then, one can use the PMNS matrix to diagonalize the light neutrino mass matrix further.

Chapter 5 describes the Type II Seesaw Mechanism by adding a $SU(2)_L$ triplet scalar Δ, which carries a hypercharge of 1 [11]. The addition of a new Yukawa interaction involving the LH lepton doublet L_i and Δ. When the neutral component of Δ gains a nonzero VEV, the nonzero neutrino mass matrix manifests, including a new scalar, which leads to new terms in the Higgs potential, including terms which violate the lepton number. The addition of the Higgs triplet leads to the manifestation of further observable decay.

Chapter 6 shows that the Type III Seesaw mechanism introduces a set of triplet leptons which generate a mass matrix similar to the Type I seesaw [12]. The addition of fermion triplets leads to the manifestation of observable decay.

The three different seesaw models can explain the manifestation of neutrino masses. However, in the Type I Seesaw, the neutrinos tend to be "sterile" as they are singlets under the SM gauge group (Unless mixed with light neutrinos). Thus, unlike the Type II and Type III Seesaw, they are difficult to detect in experiments. The triplet Higgs couples to leptons and neutrinos; therefore, in colliders, one can observe their signature decay in leptonic channels. In the Type III Seesaw, fermions carry gauge interactions, making it easier for them to be kinematically produced in colliders. The neutrino masses generated in the Type II seesaw mechanism are Majorana type. In contrast to models in which RH neutrinos include Dirac and Majorana mass terms. The presence of the Majorana mass term leads to the $0\nu\beta\beta$ decay process, which is very rare and unconfirmed. Thus, the Type II seesaw significantly depends on the $0\nu\beta\beta$ result.

8.2 Similitude of Leptogenesis Mechanisms

As demonstrated in Chapter 3, studies concerning the large-scale structure of our universe, such as the CMB and BBN, imply that the universe is predominantly made of matter. Thus, Sakharov laid down three requirements for the BAU to manifest: Baryon Number Violation, C and CP Violation, and Out of Equilibrium interactions. Through the help of the sphaleron process, if an initial lepton asymmetry exists before it occurs, the asymmetry can partially be transformed into baryon asymmetry.

Section 4.1 shows that for Type I Seesaw, the Majorana nature violates the lepton number, the CP violation comes from the Yukawa couplings, and the out-of-equilibrium requirement is given by demanding that the decay rate is less than the Hubble expansion [38]. The heavy RH neutrinos at the start of the universe would first decay predominantly into matter, which would then be transferred into BAU. At High energies (Section 7.3), Type I seesaw scenarios are difficult to experiment on as the physics has to be accessed implicitly, i.e. "falsify" potential models [69]. However, one can test the low-scale seesaw (for three quasi-degenerate Majorana neutrino models) with the upcoming $\mu^{\pm} \to e^{\pm} + \gamma$, $\mu^{\pm} \to e^{\pm} + e^{+} + e^{-}$ and $\mu - e$ conversion in nuclei experiments. Through the branching fractions of $\mu^{\pm} \to e^{\pm} + \gamma$, $\mu^{\pm} \to e^{\pm} + e^{+} + e^{-}$ and $\mu - e$ conversion in nuclei experiments, one can constraint the

parameter space of the couplings, as they are directly proportional [16]. The sensitivity of new experiments shows that μLFV experiments can directly test regions of the leptogenesis parameter space, such as in MEG II [79], Mu2e [61], COMET [62], and PRISM/PRIME [63].

Section 5.1 demonstrated that if the triplet Higgs has a non-minimal coupling with gravity and if the mixed state of the SM and triplet Higgs plays the role of inflation, then through a non-zero angular motion in the phase of the complex scalar, then an asymmetry in the lepton number density manifests [11]. At last, the asymmetry would then be transferred into BAU through sphalerons. Adding the scalar triplet Δ leads, after EWSB, to 6 new scalars in the spectrum [15]. In the scenario of Chapter 5, for a triplet Higgs VEV within the range of 0.05 eV $\lesssim v_\Delta \lesssim$ 10 keV, then the triplet Higgs will predominately decay into leptons. Colliders can search the $H^{\pm\pm}H^{\mp\mp}$ pair production in multilepton channels, and with the help of $pp \to H^{\pm\pm}H^{\mp}$ on can the sensitivity. The single-charge Higgs and doubly charged Higgs can be observed in 4-lepton, 3-lepton, and 2-lepton channels. Furthermore, below 800 GeV without a missing energy cut, one can provide a significant sensitivity in the LHC, whereas above 800 GeV $3e + E_T^{miss}$ provides a better measure of the Δ mass [15]. On the other hand, one can measure the Yukawa couplings of the triplet Higgs through the decays of $\mu^\pm \to e^\pm + \gamma$, $\mu^\pm \to e^\pm + e^+ + e^-$ and $\mu - e$ conversion in nuclei experiments [16], which further help constraint parameters in the model.

Section 6.1 finds that the Type III model (similar to the Type I seesaw) violated the lepton number by two units. Here, the decay from N_0 and $E_i^\pm$ produce the lepton number asymmetry [12]. Unlike the Type I seesaw, one can have a large efficiency factor because heavy leptons quickly decoupled from the thermal bath to decay out of equilibrium.

Overall, the three different seesaw models can explain leptogenesis. However, the Type II model requires a non-minimal coupling to gravity. The Type I model cannot be reached at high energies due to the mass of the heavy RH neutrinos. In the case of 2RHN neutrinos (Type I Low scale Seesaw), in most of the parameter regions where BAU is successful, their masses must be too degenerate to be experimentally resolved [81]. Can the 3 QD neutrino case masses be experimentally resolved? Further [82] shows that coupling to the Higgs sector of the SM can lead to dangerously large corrections to the Higgs mass in the Type II seesaw model. All three leptogenesis mechanisms rely on the sphaleron process; if changed, the calculations must be revised.

8.3 Sensitivites of Type I and Type II

As shown in Table 7.1, the most stringent experiment limits on $\mu^{\pm} \to e^{\pm} + \gamma$, $\mu^{\pm} \to e^{\pm} + e^{+} + e^{-}$ and $\mu - e$ conversion in nuclei have been reported by MEG [79], SINDRUM [54] and SINDRUM II [55] [56] collaborations.

For the Low-Scale Type I seesaw (3 QD case) and the sensitivities, one calculates that for the MEG II aiming to reach a sensitivity of $BR(\mu^{\pm} \to e^{\pm} + \gamma) \simeq 6.0 \times 10^{-14}$ [79] and using equation 7.11 and 7.12 for $M = M_W$ ($M = 1000$ GeV) one finds $\sum_{i=1,2,3} |(RV)^*_{\mu i}(RV)_{ei}| \gtrsim 3.3 \times 10^{-5}$ (8.9×10^{-6}) which less than the mas($\sum_{i=1,2,3} |(RV)^*_{\mu i}(RV)_{ei}|$) at that M, showing that one can test for leptogenesis in MEG II [14]. Mu3e, for the $BR(\mu^{\pm} \to e^{\pm} + e^{+} + e^{-})$, aims to reach a sensitivity around $10^{-15}(10^{16})$. Mu2e and COMET are trying to reach a sensitivity of Aluminium, $CR(\mu^{27}_{13}Al \to e^{27}_{13}Al)$ around 6×10^{-17}. This sensitivity can be used in equations relating branching ratios to coupling constants to achieve even smaller coupling values, leading to a better constraint. Finally, the PRISM/PRIME experiment aiming at 10^{-18} for the $\mu - e$ conversion rate in Titanium, one will find $\sum_{i=1,2,3} |(RV)^*_{\mu i}(RV)_{ei}|$ as small as 10^{-7} at $M \sim 100$ GeV [14].

For the Low-Scale Type II seesaw finds that the process, $\mu^{\pm} \to e^{\pm} + \gamma$, $\mu^{\pm} \to e^{\pm} + e^{+} + e^{-}$ and $\mu - e$ conversion in nuclei, lead to upper limits on the coupling $|(h^{\dagger}h)_{e\mu}|$ as shown in equation 7.47, 7.50 and 7.56 (respectively) [16]. These calculations have been done with sensitivities published before 2013. Given that the sensitivities in Table 7.1 for $\mu^{\pm} \to e^{\pm} + \gamma$ decay are smaller and newer, one can have more stringent upper limits on $|(h^{\dagger}h)_{e\mu}|$ from equation 7.49. Further, one can use the proposed sensitivities of MEG II, Mu2e, COMET, and PRISM/PRIME to find even more stringent upper limits on $|(h^{\dagger}h)_{e\mu}|$.

As shown in section 7.2, compared to the Crystal Box, MEGA and MEG, the sensitivity of MEG II significantly improves the limit set on the couplings form $\mu^{\pm} \to e^{\pm} + \gamma$ in the 3 QD Low Scale Seesaw.

Chapter 9

Concluding Remarks

With the addition of the Higgs field, the SM is roughly complete. However, there still remain unexplained physical phenomena, such as neutrinos and the baryon asymmetry of the universe. At first, neutrinos were modelled as massless particles, as no RH neutrino state was found in nature. However, observations of neutrino oscillations in SK [7], SNO [9], and Homestake [8] have found evidence that neutrinos do in fact have mass. To explain the neutrino mass, the "Majorana" neutrino option was introduced (where the neutrino is its own antiparticle). This inspired the extensions of the SM through the Seesaw Mechanisms. Further, modern-day experiments are looking to probe this mechanism and its parameters.

The three most widely studied Seesaw mechanisms are the Type I, II and III Seesaw models. First, in Type I, the SM is extended through additional RHN, and the SM lagrangians now include a Majorana mass term and new Yukawa interactions with the Higgs field [10]. Second, the Type II Seesaw model is extended by triplet $SU(2)_L$ scalar, which leads to the addition of a new Yukawa term and a new potential [11]. Finally, the Type III Seesaw model is extended through three LH triplets of leptons with new gauge, Yukawa and mass terms [12]. The Seesaw Mechanism, apart from explaining the neutrino mass, explains the BAU through leptogenesis. Here, either by the decay of heavy leptons or the Afflect-Dine mechanism, the universe evolves a lepton asymmetry in the early stages of existence, which is then partially transformed into baryons through a sphaleron process [38] [11] [12]. Further, leptogenesis puts constraints on the parameters proposed by Seesaw models.

The Type I Seesaw model is the most studied currently. Even though at high energies, it is shown to be difficult to probe, low-scale models are sub-TeV scale

[69], which can be probed in low-energy experiments and colliders. e.g. tests on charge lepton flavour violating muon decays can put constraints in the CC and NC couplings with the heavy Majorana neutrinos (when mixed with light neutrinos) [16]. The sensitivity of future experiments such as MEG II [79], COMET [62], and PRISM/PRIME [63] show that they will be able to test a significant portion of the region for viable leptogenesis. A positive result will serve as an indication that low-scale leptogenesis with three RH QD heavy Majorana neutrinos is preferred. A recent study of the Type II Seesaw model showed that leptogenesis is possible if a scalar Higgs triplet is added and there is a non-minimal coupling with gravity [11]. Then through the Afflect-Dine Mechanism, the BAU can be explained. The decay of the pair production of the singly charged Higgs and the doubly charged Higgs can be searched for in multilepton channels [15]. In addition, constraints on the coupling constants from tests on charge lepton flavour violating muon decays can placed. The Type II Seesaw model provides a new, unique solution to the BAU without the need for GUT or Supersymmetry.

9.1 Further Research

This investigation could be further explored by researching the current status of Type III seesaw models in regard to the collider experiments and examining their contribution to the following processes $\mu^{\pm} \rightarrow e^{\pm} + \gamma$, $\mu^{\pm} \rightarrow e^{\pm} + e^{+} + e^{-}$ and $\mu - e$ conversion in nuclei [16]. In the Type III model, both the Majorana mass eigenstates N (through the mixing with light Majorana neutrinos) and the heavy (charged) leptons E have couplings to the weak gauge bosons [16], potentially leading to corrections in the $\mu^{\pm} \rightarrow e^{\pm} + \gamma$, $\mu^{\pm} \rightarrow e^{\pm} + e^{+} + e^{-}$ and $\mu - e$ conversion in nuclei processes.

An investigation of current $0\nu\beta\beta$ searches, their constraints on seesaw models and their underlying mechanism can expand our clarification of which models work, such as a constraint of the Type II seesaw electron neutrino with only Majorana terms and an upper limit on the linear combination of neutrino masses (the $0\nu\beta\beta$ half-life is proportional to the linear combination of neutrino masses) [17]. Further, it would also be confirmation of the Majorana neutrino option, as $0\nu\beta\beta$ can only occur if a neutrino is its own antiparticle.

Further research into resonant leptogenesis, when Majorana mass are quasi-degenerate and leptogenesis via neutrino oscillations, should be further examined as they demonstrate an accessible range of parameters which can be currently tested as the heavy Majorana neutrinos can have masses sub-TeV scales [14].

Bibliography

1. Altarelli G. Collider Physics within the Standard Model: a Primer. 2013. arXiv: 1303.2842 [hep-ph]
2. Englert F and Brout R. Broken Symmetry and the Mass of Gauge Vector Mesons. Phys. Rev. Lett. 1964; 13. Ed. by Taylor JC:321–3. DOI: 10.1103/PhysRevLett.13.321
3. Guralnik GS, Hagen CR, and Kibble TWB. Global Conservation Laws and Massless Particles. Phys. Rev. Lett. 1964; 13. Ed. by Taylor JC:585–7. DOI: 10.1103/PhysRevLett.13.585
4. Higgs PW. Broken Symmetries and the Masses of Gauge Bosons. Phys. Rev. Lett. 1964; 13. Ed. by Taylor JC:508–9. DOI: 10.1103/PhysRevLett.13.508
5. Aad G et al. Observation of a new particle in the search for the Standard Model Higgs boson with the ATLAS detector at the LHC. Phys. Lett. B 2012; 716:1–29. DOI: 10.1016/j.physletb.2012.08.020. arXiv: 1207.7214 [hep-ex]
6. Goodman M. NEUTRINO PHYSICS IN 2020. *Particle Physics at the Year of Centenary of Bruno Pontecorvo*. WORLD SCIENTIFIC, 2015 Mar. DOI: 10.1142/9789814663618_0022. Available from: https://doi.org/10.1142%2F9789814663618_0022
7. Fukuda Y et al. Evidence for oscillation of atmospheric neutrinos. Phys. Rev. Lett. 1998; 81:1562–7. DOI: 10.1103/PhysRevLett.81.1562. arXiv: hep-ex/9807003
8. Cleveland BT, Daily T, Davis Jr. R, Distel JR, Lande K, Lee CK, Wildenhain PS, and Ullman J. Measurement of the solar electron neutrino flux with the Homestake chlorine detector. Astrophys. J. 1998; 496:505–26. DOI: 10.1086/305343
9. Ahmad QR et al. Direct evidence for neutrino flavor transformation from neutral current interactions in the Sudbury Neutrino Observatory. Phys. Rev. Lett. 2002; 89:011301. DOI: 10.1103/PhysRevLett.89.011301. arXiv: nucl-ex/0204008

10. Brdar V, Helmboldt AJ, Iwamoto S, and Schmitz K. Type I seesaw mechanism as the common origin of neutrino mass, baryon asymmetry, and the electroweak scale. Physical Review D 2019 Oct; 100. DOI: 10.1103/physrevd.100.075029. Available from: https://doi.org/10.1103%2Fphysrevd.100.075029
11. Barrie ND, Han C, and Murayama H. Type II Seesaw leptogenesis. Journal of High Energy Physics 2022 May; 2022. DOI: 10.1007/jhep05(2022)160. Available from: https://doi.org/10.1007%2Fjhep05%282022%29160
12. CHEN SL and HE XG. LEPTOGENESIS AND LHC PHYSICS WITH TYPE III SEE-SAW. International Journal of Modern Physics: Conference Series 2011 Jan; 01:18–27. DOI: 10.1142/s2010194511000067. Available from: https://doi.org/10.1142%2Fs2010194511000067
13. Barrow JL et al. Theories and Experiments for Testable Baryogenesis Mechanisms: A Snowmass White Paper. 2022 Mar. arXiv: 2203.07059 [hep-ph]
14. Granelli A, Klarić J, and Petcov S. Tests of low-scale leptogenesis in charged lepton flavour violation experiments. Physics Letters B 2023 Feb; 837:137643. DOI: 10.1016/j.physletb.2022.137643. Available from: https://doi.org/10.1016%2Fj.physletb.2022.137643
15. Han C, Lei Z, and Liao W. Testing type II seesaw leptogenesis at the LHC∗. Chinese Physics C 2023 Sep; 47:093104. DOI: 10.1088/1674-1137/ace708. Available from: https://doi.org/10.1088%2F1674-1137%2Face708
16. Dinh DN, Ibarra A, Molinaro E, and Petcov ST. The - e conversion in nuclei, → e, → 3e decays and TeV scale see-saw scenarios of neutrino mass generation. Journal of High Energy Physics 2012 Aug; 2012. DOI: 10.1007/jhep08(2012)125. Available from: https://doi.org/10.1007%2Fjhep08%282012%29125
17. Boyd S. Neutrino Oscillations. 2016. Available from: https://warwick.ac.uk/fac/sci/physics/staff/academic/boyd/warwick_week/neutrino_physics/lec_oscillations.pdf [Accessed on: 2023 Sep 15]
18. Abe K et al. Neutron tagging following atmospheric neutrino events in a water Cherenkov detector. JINST 2022; 17:P10029. DOI: 10.1088/1748-0221/17/10/P10029. arXiv: 2209.08609 [hep-ex]
19. Taroni A. Nobel Prize 2015: Kajita and McDonald. 2015. Available from: https://www.nature.com/articles/nphys3543 [Accessed on: 2023 Sep 15]
20. Qian X and Vogel P. Neutrino mass hierarchy. Progress in Particle and Nuclear Physics 2015 Jul; 83:1–30. DOI: 10.1016/j.ppnp.2015.05.002. Available from: https://doi.org/10.1016%2Fj.ppnp.2015.05.002

21. Klinger J. Search for heavy Majorana neutrinos in pp collisions at $\sqrt{s}$=8 TeV with the ATLAS detector. 2014. Available from: https://pure.manchester.ac.uk/ws/portalfiles/portal/54553343/FULL_TEXT.PDF [Accessed on: 2023 Sep 15]
22. RODEJOHANN W. NEUTRINO-LESS DOUBLE BETA DECAY AND PARTICLE PHYSICS. International Journal of Modern Physics E 2011 Sep; 20:1833–930. DOI: 10.1142/s0218301311020186. Available from: https://doi.org/10.1142%2Fs0218301311020186
23. Seljak U et al. Cosmological parameter analysis including SDSS Ly-alpha forest and galaxy bias: Constraints on the primordial spectrum of fluctuations, neutrino mass, and dark energy. Phys. Rev. D 2005; 71:103515. DOI: 10.1103/PhysRevD.71.103515. arXiv: astro-ph/0407372
24. Komatsu E et al. Five-Year Wilkinson Microwave Anisotropy Probe (WMAP) Observations: Cosmological Interpretation. Astrophys. J. Suppl. 2009; 180:330–76. DOI: 10.1088/0067-0049/180/2/330. arXiv: 0803.0547 [astro-ph]
25. Kneller JP and Steigman G. BBN for pedestrians. New J. Phys. 2004; 6:117. DOI: 10.1088/1367-2630/6/1/117. arXiv: astro-ph/0406320
26. Fields B and Sarkar S. Big-Bang nucleosynthesis (2006 Particle Data Group mini-review). 2006 Jan. arXiv: astro-ph/0601514
27. Sousa Seixas D de. Massive Neutrinos and Leptogenesis. 2009. Available from: https://fenix.tecnico.ulisboa.pt/downloadFile/395139377913/TeseDavidSeixas.pdf [Accessed on: 2023 Sep 16]
28. Sakharov AD. Violation of CP Invariance, C asymmetry, and baryon asymmetry of the universe. Pisma Zh. Eksp. Teor. Fiz. 1967; 5:32–5. DOI: 10.1070/PU1991v034n05ABEH002497
29. K.S.Lim. Introduction to Baryogenesis and Leptogenesis. 2011. Available from: https://www.mpi-hd.mpg.de/lin/events/group_seminar/inflation/lim.pdf [Accessed on: 2023 Sep 16]
30. Marion GG van. Sphalerons and the Vacuum Structure of Gauge Theories. 2020. Available from: https://fse.studenttheses.ub.rug.nl/22678/1/mPHYS_2020_vanMarionGG.pdf [Accessed on: 2023 Sep 16]
31. Pontecorvo B. Inverse beta processes and nonconservation of lepton charge. Zh. Eksp. Teor. Fiz. 1957; 34:247
32. Maki Z, Nakagawa M, and Sakata S. Remarks on the unified model of elementary particles. Prog. Theor. Phys. 1962; 28:870–80. DOI: 10.1143/PTP.28.870
33. Esteban I, Gonzalez-Garcia MC, Hernandez-Cabezudo A, Maltoni M, and Schwetz T. Global analysis of three-flavour neutrino oscillations: synergies

and tensions in the determination of 23, CP, and the mass ordering. Journal of High Energy Physics 2019 Jan; 2019. DOI: 10.1007/jhep01(2019)106. Available from: https://doi.org/10.1007%2Fjhep01%282019%29106

34. Abe K et al. Atmospheric neutrino oscillation analysis with external constraints in Super-Kamiokande I-IV. Phys. Rev. D 2018; 97:072001. DOI: 10.1103/PhysRevD.97.072001. arXiv: 1710.09126 [hep-ex]
35. NuFit. 2018. Available from: http://www.nu-fit.org/ [Accessed on: 2023 Sep 16]
36. Casas JA and Ibarra A. Oscillating neutrinos and $\mu \to e, \gamma$. Nucl. Phys. B 2001; 618:171–204. DOI: 10.1016/S0550-3213(01)00475-8. arXiv: hep-ph/0103065
37. Fukugita M and Yanagida T. Baryogenesis Without Grand Unification. Phys. Lett. B 1986; 174:45–7. DOI: 10.1016/0370-2693(86)91126-3
38. Fong CS, Nardi E, and Riotto A. Leptogenesis in the Universe. Adv. High Energy Phys. 2012; 2012:158303. DOI: 10.1155/2012/158303. arXiv: 1301.3062 [hep-ph]
39. Flanz M, Paschos EA, and Sarkar U. Baryogenesis from a lepton asymmetric universe. Physics Letters B 1995 Feb; 345:248–52. DOI: 10.1016/0370-2693(94)01555-q. Available from: https://doi.org/10.1016%2F0370-2693%2894%2901555-q
40. Harvey JA and Turner MS. Cosmological baryon and lepton number in the presence of electroweak fermion-number violation. Phys. Rev. D 1990 Nov; 42(10):3344–9. DOI: 10.1103/PhysRevD.42.3344. Available from: https://link.aps.org/doi/10.1103/PhysRevD.42.3344
41. Aaboud M et al. Search for doubly charged Higgs boson production in multi-lepton final states with the ATLAS detector using proton–proton collisions at $\sqrt{s} = 13\,\text{TeV}$. Eur. Phys. J. C 2018; 78:199. DOI: 10.1140/epjc/s10052-018-5661-z. arXiv: 1710.09748 [hep-ex]
42. Kanemura S and Yagyu K. Radiative corrections to electroweak parameters in the Higgs triplet model and implication with the recent Higgs boson searches. Physical Review D 2012 Jun; 85. DOI: 10.1103/physrevd.85.115009. Available from: https://doi.org/10.1103%2Fphysrevd.85.115009
43. Affleck I and Dine M. A New Mechanism for Baryogenesis. Nucl. Phys. B 1985; 249:361–80. DOI: 10.1016/0550-3213(85)90021-5
44. Cai Y, Han T, Li T, and Ruiz R. Lepton Number Violation: Seesaw Models and Their Collider Tests. 2018. arXiv: 1711.02180 [hep-ph]

45. Pilaftsis A and Underwood TE. Resonant leptogenesis. Nuclear Physics B 2004 Aug; 692:303–45. DOI: 10.1016/j.nuclphysb.2004.05.029. Available from: https://doi.org/10.1016%2Fj.nuclphysb.2004.05.029
46. Granelli A, Moffat K, and Petcov S. Flavoured resonant leptogenesis at sub-TeV scales. Nuclear Physics B 2021 Dec; 973:115597. DOI: 10.1016/j.nuclphysb.2021.115597. Available from: https://doi.org/10.1016%2Fj.nuclphysb.2021.115597
47. Akhmedov EK, Rubakov VA, and Smirnov AY. Baryogenesis via Neutrino Oscillations. Physical Review Letters 1998 Aug; 81:1359–62. DOI: 10.1103/physrevlett.81.1359. Available from: https://doi.org/10.1103%2Fphysrevlett.81.1359
48. Klarić J, Shaposhnikov M, and Timiryasov I. Uniting Low-Scale Leptogenesis Mechanisms. Physical Review Letters 2021 Sep; 127. DOI: 10.1103/physrevlett.127.111802. Available from: https://doi.org/10.1103%2Fphysrevlett.127.111802
49. Drewes M, Georis Y, and Klarić J. Mapping the Viable Parameter Space for Testable Leptogenesis. Phys. Rev. Lett. 2022; 128:051801. DOI: 10.1103/PhysRevLett.128.051801. arXiv: 2106.16226 [hep-ph]
50. Blennow M, Coloma P, Fernandez-Martinez E, Hernandez-Garcia J, and Lopez-Pavon J. Non-unitarity, sterile neutrinos, and non-standard neutrino interactions. Journal of High Energy Physics 2017 Apr; 2017. DOI: 10.1007/jhep04(2017)153. Available from: https://doi.org/10.1007%2Fjhep04%282017%29153
51. Fernandez-Martinez E, Hernandez-Garcia J, Lopez-Pavon J, and Lucente M. Loop level constraints on Seesaw neutrino mixing. Journal of High Energy Physics 2015 Oct; 2015. DOI: 10.1007/jhep10(2015)130. Available from: https://doi.org/10.1007%2Fjhep10%282015%29130
52. Tanabashi M et al. Review of Particle Physics. Phys. Rev. D 2018; 98:030001. DOI: 10.1103/PhysRevD.98.030001
53. Collaboration TM. Search for the Lepton Flavour Violating Decay $\mu^+ \to e^+\gamma$ with the Full Dataset of the MEG Experiment. 2016. arXiv: 1605.05081 [hep-ex]
54. Eichler R and Grab C. The SINDRUM-I Experiment. SciPost Phys. Proc. 2021; 5:007. DOI: 10.21468/SciPostPhysProc.5.007
55. Dohmen C et al. Test of lepton flavor conservation in mu —> e conversion on titanium. Phys. Lett. B 1993; 317:631–6. DOI: 10.1016/0370-2693(93)91383-X

56. Bertl WH et al. A Search for muon to electron conversion in muonic gold. Eur. Phys. J. C 2006; 47:337–46. DOI: 10.1140/epjc/s2006-02582-x

57. Alonso R, Dhen M, Gavela MB, and Hambye T. Muon conversion to electron in nuclei in type-I seesaw models. JHEP 2013; 01:118. DOI: 10.1007/JHEP01(2013)118. arXiv: 1209.2679 [hep-ph]

58. Ibarra A, Molinaro E, and Petcov ST. Low energy signatures of the TeV scale seesaw mechanism. Physical Review D 2011 Jul; 84. DOI: 10.1103/physrevd.84.013005. Available from: https://doi.org/10.1103%2Fphysrevd.84.013005

59. Baldini AM, Baracchini E, Bemporad C, Berg F, Biasotti M, Boca G, Cattaneo PW, Cavoto G, Cei F, Chiappini M, Chiarello G, Chiri C, Cocciolo G, Corvaglia A, Bari A de, Gerone MD, D'Onofrio A, Francesconi M, Fujii Y, Galli L, Gatti F, Grancagnolo F, Grassi M, Grigoriev DN, Hildebrandt M, Hodge Z, Ieki K, Ignatov F, Iwai R, Iwamoto T, Kaneko D, Kasami K, Kettle PR, Khazin BI, Khomutov N, Korenchenko A, Kravchuk N, Libeiro T, Maki M, Matsuzawa N, Mihara S, Milgie M, Molzon W, Mori T, Morsani F, Mtchedilishvili A, Nakao M, Nakaura S, Nicolò D, Nishiguchi H, Nishimura M, Ogawa S, Ootani W, Panareo M, Papa A, Pepino A, Piredda G, Popov A, Raffaelli F, Renga F, Ripiccini E, Ritt S, Rossella M, Rutar G, Sawada R, Signorelli G, Simonetta M, Tassielli GF, Uchiyama Y, Usami M, Venturini M, Voena C, Yoshida K, Yudin YV, and Zhang Y. The design of the MEG II experiment. The European Physical Journal C 2018 May; 78. DOI: 10.1140/epjc/s10052-018-5845-6. Available from: https://doi.org/10.1140%2Fepjc%2Fs10052-018-5845-6

60. Arndt K et al. Technical design of the phase I Mu3e experiment. Nucl. Instrum. Meth. A 2021; 1014:165679. DOI: 10.1016/j.nima.2021.165679. arXiv: 2009.11690 [physics.ins-det]

61. Bartoszek L et al. Mu2e Technical Design Report. 2014 Oct. DOI: 10.2172/1172555. arXiv: 1501.05241 [physics.ins-det]

62. Abramishvili R et al. COMET Phase-I Technical Design Report. PTEP 2020; 2020:033C01. DOI: 10.1093/ptep/ptz125. arXiv: 1812.09018 [physics.ins-det]

63. Barlow R. The PRISM/PRIME Project. Nuclear Physics B - Proceedings Supplements 2011; 218. Proceedings of the Eleventh International Workshop on Tau Lepton Physics:44–9. DOI: https://doi.org/10.1016/j.nuclphysbps.2011.06.009. Available from: https://www.sciencedirect.com/science/article/pii/S0920563211005330

64. Chrzaszcz M, Drewes M, Gonzalo TE, Harz J, Krishnamurthy S, and Weniger C. A Frequentist analysis of three right-handed neutrinos with GAMBIT. The European Physical Journal C 2020 Jun; 80. DOI: 10.1140/epjc/s10052-020-8073-9. Available from: https://doi.org/10.1140%2Fepjc%2Fs10052-020-8073-9

65. Aubert B et al. Searches for Lepton Flavor Violation in the Decays tau+- —> e+- gamma and tau+- —> mu+- gamma. Phys. Rev. Lett. 2010; 104:021802. DOI: 10.1103/PhysRevLett.104.021802. arXiv: 0908.2381 [hep-ex]

66. Hayasaka K et al. Search for Lepton Flavor Violating Tau Decays into Three Leptons with 719 Million Produced Tau+Tau- Pairs. Phys. Lett. B 2010; 687:139–43. DOI: 10.1016/j.physletb.2010.03.037. arXiv: 1001.3221 [hep-ex]

67. Renga F. Experimental searches for muon decays beyond the Standard Model. Reviews in Physics 2019; 4:100029. DOI: https://doi.org/10.1016/j.revip.2019.100029. Available from: https://www.sciencedirect.com/science/article/pii/S2405428318300601

68. Collaboration M, Brooks M, Chen Y, Cooper M, Cooper P, Dzemidzic M, Empl A, Gagliardi C, Hogan G, Hughes E, et al. New Limit for the Family-Number Non-conserving Decay mu+ to e+ _gamma. arXiv preprint hep-ex/9905013 1999

69. Barrow JL, Broussard L, Cline JM, Dev PSB, Drewes M, Elor G, Gardner S, Ghiglieri J, Harz J, Kamyshkov Y, Klaric J, Koerner LW, Laurent B, McGehee R, Postma M, Shakya B, Shrock R, Vis J van de, and White G. Theories and Experiments for Testable Baryogenesis Mechanisms: A Snowmass White Paper. 2022. arXiv: 2203.07059 [hep-ph]

70. Klapdor-Kleingrothaus HV, Dietz A, Harney HL, and Krivosheina IV. Evidence for neutrinoless double beta decay. Mod. Phys. Lett. A 2001; 16:2409–20. DOI: 10.1142/S0217732301005825. arXiv: hep-ph/0201231

71. Arnold R et al. Results of the search for neutrinoless double-β decay in ^{100}Mo with the NEMO-3 experiment. Phys. Rev. D 2015; 92:072011. DOI: 10.1103/PhysRevD.92.072011. arXiv: 1506.05825 [hep-ex]

72. Agostini M et al. Final Results of GERDA on the Search for Neutrinoless Double-β Decay. Phys. Rev. Lett. 2020; 125:252502. DOI: 10.1103/PhysRevLett.125.252502. arXiv: 2009.06079 [nucl-ex]

73. A search for doubly-charged Higgs boson production in three and four lepton final states at $\sqrt{s} = 13$ TeV. 2017

74. Muhlleitner M and Spira M. A Note on doubly charged Higgs pair production at hadron colliders. Phys. Rev. D 2003; 68:117701. DOI: 10.1103/PhysRevD.68.117701. arXiv: hep-ph/0305288

75. Fileviez Perez P, Han T, Huang Gy, Li T, and Wang K. Neutrino Masses and the CERN LHC: Testing Type II Seesaw. Phys. Rev. D 2008; 78:015018. DOI: 10.1103/PhysRevD.78.015018. arXiv: 0805.3536 [hep-ph]

76. Aad G et al. Search for doubly charged Higgs boson production in multi-lepton final states using 139 fb^{-1} of proton–proton collisions at $\sqrt{s} = 13$ TeV with the ATLAS detector. Eur. Phys. J. C 2023; 83:605. DOI: 10.1140/epjc/s10052-023-11578-9. arXiv: 2211.07505 [hep-ex]

77. Junk T. Confidence level computation for combining searches with small statistics. Nucl. Instrum. Meth. A 1999; 434:435–43. DOI: 10.1016/S0168-9002(99)00498-2. arXiv: hep-ex/9902006

78. Campbell JM, Ellis RK, and Williams C. Vector boson pair production at the LHC. JHEP 2011; 07:018. DOI: 10.1007/JHEP07(2011)018. arXiv: 1105.0020 [hep-ph]

79. Adam J et al. New limit on the lepton-flavour violating decay $\mu^+ \to e^+\gamma$. Phys. Rev. Lett. 2011; 107:171801. DOI: 10.1103/PhysRevLett.107.171801. arXiv: 1107.5547 [hep-ex]

80. Kitano R, Koike M, and Okada Y. Detailed calculation of lepton flavor violating muon electron conversion rate for various nuclei. Phys. Rev. D 2002; 66. [Erratum: Phys.Rev.D 76, 059902 (2007)]:096002. DOI: 10.1103/PhysRevD.76.059902. arXiv: hep-ph/0203110

81. Drewes M, Garbrecht B, Gueter D, and Klaric J. Testing the low scale seesaw and leptogenesis. JHEP 2017; 08:018. DOI: 10.1007/JHEP08(2017)018. arXiv: 1609.09069 [hep-ph]

82. Dev PSB, Vila CM, and Rodejohann W. Naturalness in testable type II seesaw scenarios. Nucl. Phys. B 2017; 921:436–53. DOI: 10.1016/j.nuclphysb.2017.06.007. arXiv: 1703.00828 [hep-ph]